LAPPEENRANTA UNIVERSITY OF TECHNOLOGY
LUT School of Energy Systems
Degree Programme in Energy Technology

Anu-Maria Olli

CONTROL OF BUBBLING FLUIDIZED BED CONDITIONS

Master's Thesis 2016

Examiners: Professor, Ph.D. Esa Vakkilainen
Research Assistant, M.Sc. (Tech.) Kari Luostarinen
Supervisor: M.Sc. (Tech.) Antti Rossi

ABSTRACT

Lappeenranta University of Technology
LUT School of Energy Systems
Degree Programme in Energy Technology

Anu-Maria Olli

Control of Bubbling Fluidized Bed Conditions

Master's Thesis
2016
78 pages, 39 figures, 11 tables

Examiners: Professor, Ph.D. Esa Vakkilainen
Research Assistant, M.Sc. (Tech.) Kari Luostarinen
Supervisor: M.Sc. (Tech.) Antti Rossi
Keywords: BFB boiler, bubbling fluidized bed, agglomeration, acoustic emission, digital image processing

The objectives of this master's thesis were to understand the importance of bubbling fluidized bed (BFB) conditions and to find out how digital image processing and acoustic emission technology can help in monitoring the bed quality. An acoustic emission (AE) measurement system and a bottom ash camera system were evaluated in acquiring information about the bed conditions.

The theory part of the study describes the fundamentals of BFB boiler and evaluates the characteristics of bubbling bed. Causes and effects of bed material coarsening are explained. The ways and methods to monitor the behaviour of BFB are determined. The study introduces the operating principles of AE technology and digital image processing.

The empirical part of the study describes an experimental arrangement and results of a case study at an industrial BFB boiler. Sand consumption of the boiler was reduced by optimization of bottom ash handling and sand feeding. Furthermore, data from the AE measurement system and the bottom ash camera system was collected. The feasibility of these two systems was evaluated. The particle size of bottom ash and the changes in particle size distribution were monitored during the test period.

Neither of the systems evaluated was ready to serve in bed quality control accurately or fast enough. Particle size distributions according to the bottom ash camera did not correspond to the results of manual sieving. Comprehensive interpretation of the collected AE data requires much experience. Both technologies do have potential and with more research and development they may enable acquiring reliable and real-time information about the bed conditions. This information could help to maintain disturbance-free combustion process and to optimize bottom ash handling system.

TIIVISTELMÄ

Lappeenrannan teknillinen yliopisto
LUT School of Energy Systems
Energiatekniikan koulutusohjelma

Anu-Maria Olli
Kuplapetin olosuhteiden valvonta

Diplomityö
2016
78 sivua, 39 kuvaa, 11 taulukkoa

Tarkastajat: Professori, TkT Esa Vakkilainen
Tutkimusassistentti, DI Kari Luostarinen
Ohjaaja: DI Antti Rossi
Hakusanat: kuplapetikattila, kupliva leijupeti, sintraus, akustinen emissio, digitaalinen kuvankäsittely

Tämän diplomityön tavoitteena oli ymmärtää, mikä merkitys kuplapetin olosuhteilla on ja selvittää, miten digitaalinen kuvankäsittely ja akustinen emissio voivat auttaa petin laadunvalvonnassa. Työssä arvioitiin akustisen emission (AE) mittausjärjestelmän ja pohjatuhkakamerasovelluksen käyttökelpoisuutta kuplapetin olosuhteiden valvonnassa.

Työn teoriaosassa kuvataan kuplapetikattilan tekniikkaa ja kuplivan leijupetin ominaispiirteitä. Lisäksi selvitetään petimateriaalin karkenemisen syitä ja seurauksia. Työssä kuvaillaan kuplapetin valvomiseen käytössä olevia keinoja ja menetelmiä. Lisäksi esitellään AE tekniikan ja digitaalisen kuvankäsittelyn toimintaperiaatteita.

Työn kokeellisessa osassa kuvataan tehty koejärjestely eräällä teollisuuden kuplapetikattilalla ja esitetään kokeissa saadut tulokset. Hiekankulutusta vähennettiin optimoimalla pohjatuhkankäsittely- ja hiekansyöttöjärjestelmiä. Kokeiden aikana kerättiin dataa AE mittausjärjestelmästä ja pohjatuhkakamerasovelluksesta. Lisäksi arvioitiin sovellusten käyttökelpoisuutta kuplapetin valvonnassa. Pohjatuhkan partikkelikokoa ja muutoksia partikkelikokojakaumassa valvottiin koejakson ajan.

Kumpikaan sovelluksista ei ollut sellaisenaan valmis valvomaan petin kuntoa riittävällä tarkkuudella tai nopeudella. Pohjatuhkakameran määrittämä partikkelikokojakauma ei vastannut manuaalisen seulonnan tuloksia. Kokonaisvaltainen AE datan tulkinta vaatii paljon kokemusta. Molemmilla teknologioilla on potentiaalia. Tutkimuksen ja kehityksen avulla ne voivat tulevaisuudessa mahdollistaa luotettavan ja reaaliaikaisen tiedonsaannin kuplapetin olosuhteista. Tieto petistä auttaisi ylläpitämään häiriötöntä palamisprosessia ja optimoimaan pohjatuhkankäsittelyjärjestelmää.

ACKNOWLEDGEMENTS

The work presented in this master's thesis has been carried out as a commission of Andritz Oy.

First of all, I wish to express my gratitude to my supervisor Antti Rossi for his helpful guidance, honest feedback and encouraging support throughout the work. I am grateful to him especially for introducing me to coding and digital image processing. I would like to thank the colleagues at Andritz Oy who have shared the knowledge and tools that made this project possible. I wish to thank Professor Esa Vakkilainen for his always so speedy feedback and help.

I would like to thank my friends and family for their support throughout my studies in Lappeenranta. Special thanks go to my dearest Petri for brightening my everyday life and tirelessly reminding me that þetta reddast.

Varkaus, the 16th of May 2016

Anu-Maria Olli

TABLE OF CONTENTS

NOMENCLATURE

Latin letters

Ar	Archimedes number	[-]
d	diameter	[m]
g	standard gravity	[m/s^2]
p	pressure	[Pa, bar]
Re	Reynolds number	[-]
U	fluid velocity	[m/s]

Greek letters

ε	volume fraction of gas	[-]
μ	dynamic viscosity	[kg/ms]
ρ	density	[kg/m^3]
φ	particle sphericity	[-]

Subscripts

g	gas
mb	minimum bubbling
mf	minimum fluidization
s	solid
t	terminal

Abbreviations

AE	Acoustic Emission
BFB	Bubbling Fluidized Bed
CFB	Circulating Fluidized Bed
daf	Dry and Ash Free
db	Dry Based
DCS	Distributed Control System
FFT	Fast Fourier Transform
FW	Front Wall
IDE	Integrated Development Environment
LHV	Lower Heating Value
NDT	Non-Destructive Testing
OpenCV	Open Source Computer Vision

RDF	Refuse-Derived Fuel
RW	Rear Wall
TDH	Transport Disengaging Height

1 INTRODUCTION

The use of fluidized bed technology began in the chemical industry in the 1920's. First the technology was applied in oil cracking and coal gasification. Soon fluidized beds were utilized in multiple applications in chemical and metallurgical industries. First fluidized bed boilers were designed and constructed in the 1970's. Since then fluidized bed boilers have enabled environmentally friendly combustion of solid fuels. The technology is suitable especially for low-grade fuels, like biomasses, that have rapid changes in quality. (Blomberg 2005, 45.)

Originally coal has been the fuel burned in fluidized beds. Biomass has offered an alternative for fossil fuels in more sustainable energy production. Use of renewable biomasses aims at reduction of carbon dioxide (CO_2) emissions. Combustion of biomass can bring on some technical challenges that should be taken into consideration. These include nitrogen oxides (NO_x) and dust emissions, slagging, fouling and corrosion on heat-exchange surfaces. (Khan et al. 2009, 21–23.)

Bubbling Fluidized Bed (BFB) boiler technology has many advantages. In BFB boilers it is possible to burn different kind of fuels from biomasses to municipal waste with low emissions and high combustion efficiency. The technology allows rapid changes in fuel quality. Along with many advantages fluidized bed combustion technology has some challenges. Variation in fuel quality causes variations in fuel feed and combustion properties. Especially impurities in fuel tend to cause problems. This may increase emissions and reduce combustion efficiency. Changes in fuel quality can also cause rapid changes in steam load. (Hyppänen & Raiko 2002, 490–491; Teir 2003, 38.)

The core in overcoming the challenges in fluidization and combustion is to know and understand the bed behaviour. The control of bed conditions can improve boiler operation in both economic and environmental ways. Real-time information about BFB conditions helps in preventing disturbances in the process that can ultimately lead to unplanned shutdowns. These disturbances include incomplete mixing and combustion, bed sintering and slagging. With knowledge and understanding about the bed, it is also possible to optimize the consumption of fresh bed material.

1.1 Objectives of the Study

The base of the study is built on the understanding of fluidization theory, biomass combustion and bed behaviour in BFB boiler. The main objective is to understand the operating principles and evaluate the feasibility of two applications in the control of bubbling bed quality. These applications include acoustic emission (AE) measurements in the bed and image analysis from the bottom ash. In the empirical study another objective was to optimize the consumption of fresh bed material and the use of bottom ash handling system at an industrial BFB boiler.

This thesis endeavours to answer to the following questions:

1. Why is it important to get information about the bubbling bed conditions?
2. How can digital image processing and AE measurement help in monitoring of BFB conditions?
3. What to consider when using these technologies in acquiring knowledge of BFB conditions?

1.2 Scope and Structure of the Thesis

This master's thesis deals with BFB boilers burning biomasses, producing steam and used in electricity and/or heat production. The study concentrates on acoustic emission technology and digital image processing as tools in monitoring of bed quality. In the theory part of the thesis scientific literature and previous research is studied and demonstrated with examples. The empirical part of the thesis is a case study at an industrial BFB boiler. It evaluates two applications that offer tools for acquiring knowledge of bed conditions.

The thesis is constructed from 7 chapters. After introduction the fundamentals of BFB boiler is presented in chapter 2. Chapter 3 evaluates the characteristics of bubbling bed and describes ways and methods to monitor the behaviour of BFB. Chapter 4 introduces acoustic emission measurements and chapter 5 digital image processing in monitoring of bed conditions. Chapter 6 describes an experimental arrangement and results of a case study at an industrial BFB boiler. The case study concentrates on the reduction of sand consumption and monitoring the particle size of bottom ash. Finally, the 7th chapter concludes and summarises the study by evaluating the results and contemplating the future research.

2 BUBBLING FLUIDIZED BED BOILER

BFB boiler consists of a furnace and a convective heat exchange part like any conventional boiler. The main function of a BFB boiler is to evaporate water and further superheat the produced steam. Superheated steam can be utilized in power and/or heat production and in separate industrial processes. Flue gases are combustion products that form in combustion chamber. Flue gases flow from the furnace to back-pass(es) and through flue gas duct, dust filter, fan and finally stack. On the way heat from the flue gases is transferred to steam, water and combustion air.

Figure 1 portrays a biomass boiler with its main components and systems marked. This kind of a boiler has natural water/steam circulation. It is based on the density differences between the water and steam mixtures in downcomers (higher density) and wall tubes (lower density). Water and steam circulation can be divided into three stages: preheating, evaporation and superheating. (Teir 2003, 54–61.)

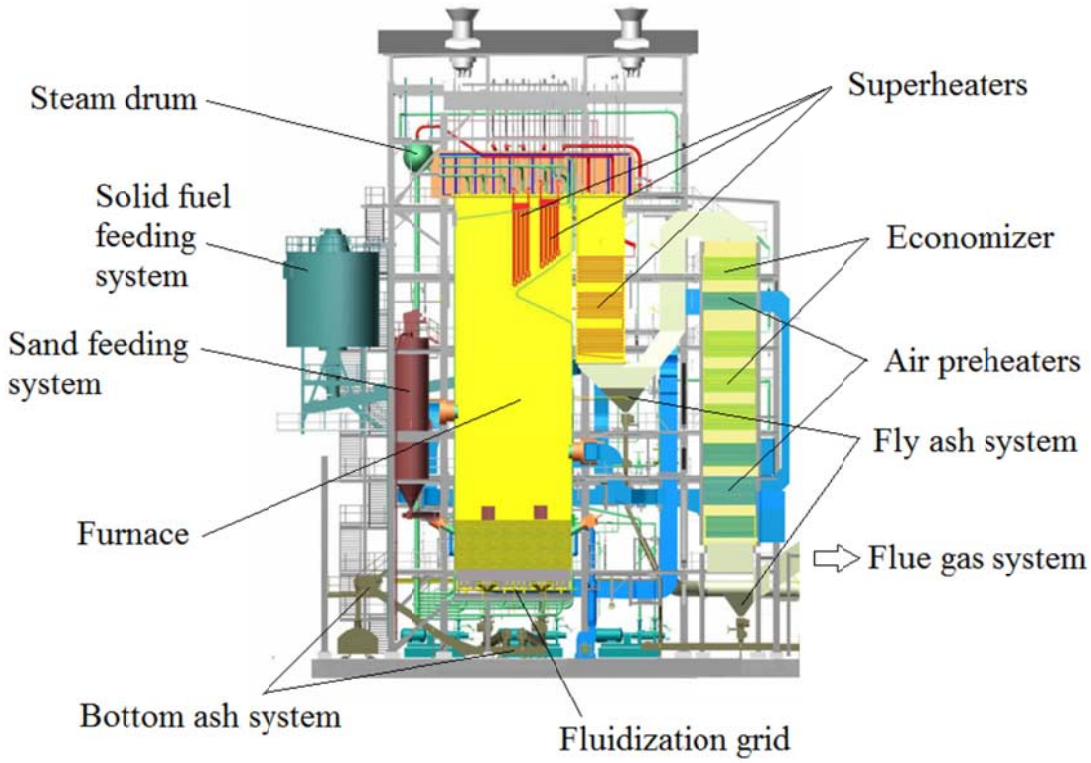

Figure 1. Main components and systems of a bubbling fluidized bed boiler are marked. (from Andritz Oy 2016.)

Water from the feed water tank is pumped to the economizer that preheats the water. Preheated water flows to the steam drum where feed water is mixed with boiler water. Downcomers move saturated water from the steam drum to distributing header. From there water flows to the wall tubes and furnace grid tubes. Water starts to evaporate. From the wall tubes the mixture of water and steam returns to the steam drum where steam is separated from water. Saturated steam flows to superheaters and saturated water returns to evaporation. In superheaters steam is heated beyond the temperature of saturated steam. Superheating increases the energy production efficiency. (Teir 2003, 54–61, 73–76, 107–109.)

2.1 Fluidization and Bed Hydrodynamics

Fluidization can be defined as

> *"the operation through which fine solids are transformed into a fluid like state through contact with a gas or liquid"* (Basu 2006, 21).

In fluidized bed gas is blown through a bed of granular material. The bed has similar characteristics as a fluid. It is essential to understand the hydrodynamics of fluidized bed because the gas-solid motion results in the environmental and operating characteristics of the bed. In BFB combustion solid fuel, combustion air, bed material and ash together form an emulsion. (Basu 2006, 21.) As the fluidization air velocity increases, motion of the particles changes. Fluidization regimes are classified in order of increasing gas velocity:

- fixed bed (stoker), relative to each other particles do not move
- bubbling bed (BFB), bed starts to behave like a fluid
- turbulent bed
- fast bed (circulating fluidized bed, CFB)
- transport bed (pulverized coal). (Basu 2006, 21–29.)

Minimum fluidization velocity of gas, U_{mf}, is the gas velocity needed to achieve fluidization. At this velocity constant contact between bed particles stops and particles start to move. Bed starts to expand and behave like a fluid. While the velocity increases and reaches minimum bubbling velocity, U_{mb}, gas bubbles start to form and rise up. The

bubbles start to disappear when the gas velocity approaches the terminal velocity of a particle, U_t. The terminal velocity of a particle is an equilibrium velocity the particle reaches after been let fallen freely. Terminal velocity is the maximal fluidization velocity. Above it, fluidized regime turns from bubbling regime into turbulent. (Basu 2006, 21–29.)

Value of U_{mf} depends on the particle size and material. Minimum fluidizing velocity can be solved through iteration from equations (1) (2) and (3). There are several correlations for U_{mf} in the literature that are modifications of equation (1) determined empirically. U_{mf} is an important design value used in modelling of fluidization and combustion. It depends on the properties and particle size of bed material. (Hyppänen & Raiko 2002, 495–498.)

$$\frac{150(1-\varepsilon_{mf})}{\varepsilon_{mf}^3 \varphi^2}\mathrm{Re}_{mf} + \frac{1.75}{\varepsilon_{mf}^3 \varphi}\mathrm{Re}_{mf}^2 = \mathrm{Ar} \tag{1}$$

When Reynolds number and Archimedes number are defined as follows:

$$\mathrm{Re}_{mf} = \frac{d_p U_{mf} \rho_g}{\mu_g} \tag{2}$$

$$\mathrm{Ar} = \frac{d_p^3 \rho_g (\rho_s - \rho_g) g}{\mu_g^2} \tag{3}$$

Behaviour and mass transfer of a BFB can be described with two-phase flow model. Fluidization gas flows through the bed in emulsion phase and bubble phase as seen in Figure 2. Emulsion phase is constantly at the minimum fluidization state while the excess gas flow forms bubbles. (Hyppänen & Raiko 2002, 500–504.)

Bubbles in the bubbling bed consist of gas and little solids. Gas usually enters a bubble from the bottom and leaves from the top. The bubble rises in the bed because of the linearly decreasing static pressure outside the bubble when moving from the bottom to the top of the bed. The pressure inside the bubble at a certain height is constant. At the top of the bubble the pressure is greater and at the bottom greater than in its surroundings. The bubble can eject solids into the freeboard when it erupts at the top of the bed. Bubbles can

grow to a maximum size and bubbles bigger than that will collapse. Bubble size depends on solid particle size, excess gas velocity and its distance above the bottom of the bed. (Basu 2006, 21–28.)

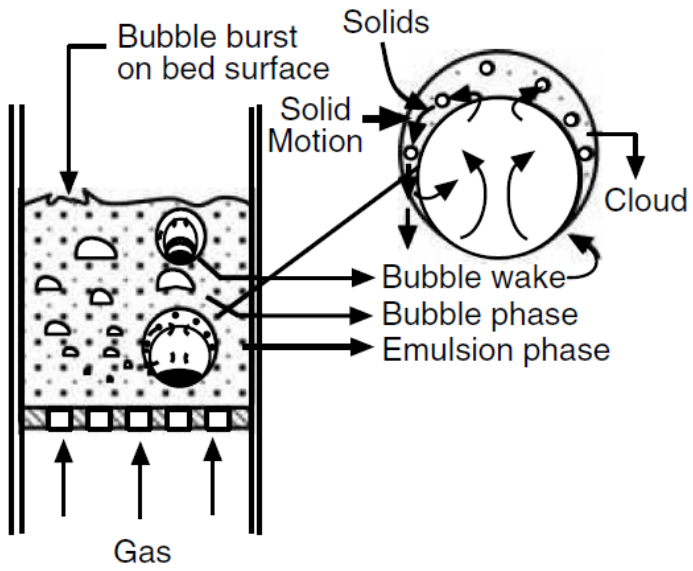

Figure 2. Bubbling bed regime has two phases: emulsion and bubbles. Gas circulation around a bubble mixes solid particles. (from Basu 2006, 23.)

Particle size distribution has a remarkable influence on the hydrodynamics. Geldart (1973, 285–287) has divided fluidization behaviour into four groups depending on the particle size and the density differences between solid particles and gas. Classification describes fluidization properties of different kind of particles. These four particle groups have properties as follows:

Group C: Very fine particles that are cohesive. Fluidization is extremely difficult because of strong inter-particle forces. Particles will not mix well and heat transfer between the bed and a surface is poor.

Group A: Small particles and/or low density particles. Particles fluidize well. They expand significantly before bubbling starts. The gas velocity needs to rise considerably over the minimum fluidization velocity for the bed to bubble.

Group B: Most of the fluidized beds use this group of particles, e.g. sand. Particles fluidize well. In contrast to Group A particles, bed expansion is smaller. Bubbling starts as soon as the minimum fluidization velocity exceeds.

Group D: Large and/or high density particles. Coarse particles require high velocity to fluidize and bubble. Bubbles are big and fluidization is harder to control than with Group B particles. (Geldart 1973, 285–287; Basu 2006, 442–444.)

Geldart's chart, presented in Figure 3, helps in evaluating a material's suitability to fluidize. BFB boilers operate usually on group B particles. Medium size of bed material particles in BFB is typically 1 millimetre and fluidization velocity can be 1–3 metres per second (Hyppänen & Raiko 2002, 490).

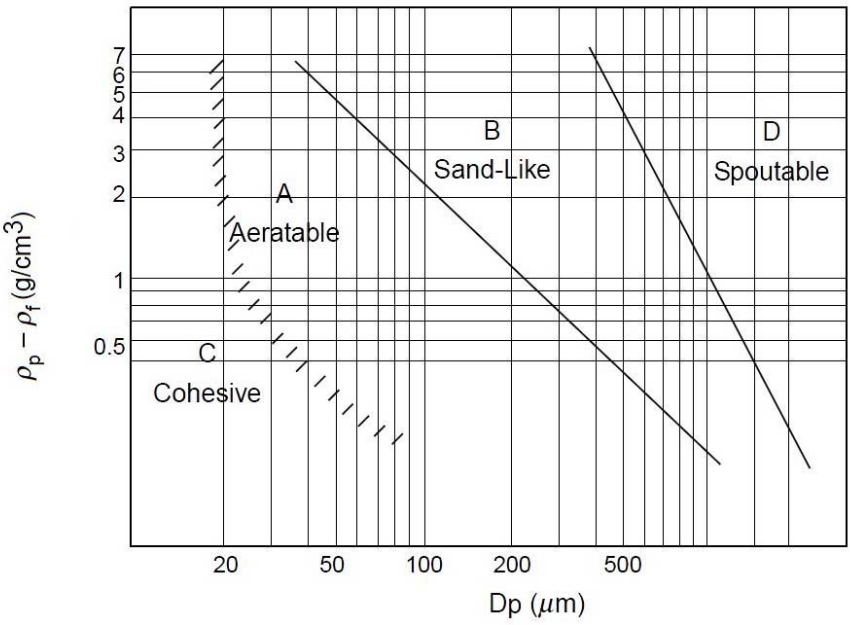

Figure 3. Geldart's grouping of particle fluidization depends on particle size and density. (Basu 2006, 443.)

The furnace of a BFB boiler can be divided horizontally into regions by concentration of solid particles. This is portrayed in Figure 4. Furnace consists of bed and freeboard above it. The splash zone is a region immediately above the bubbling bed. Transport disengaging height (TDH) is the height at which almost none of the entered solid particles return to bubbling bed. Above the TDH density of solid particles is constant. (Basu 2006, 21–28.)

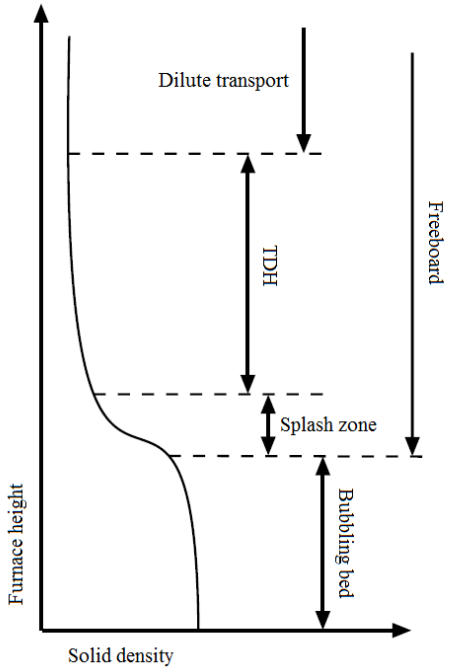

Figure 4. The furnace of BFB boiler can be divided into horizontal regions by the solid concentration. (from Basu 2006, 26.)

2.2 Biomass Fuels and Combustion in a BFB

The most general biomass fuels used in BFB's include

- wood fuels (such as hard and soft wood, demolition wood)
- herbaceous fuels (straw, grass)
- waste fuels (sludges, RDF)
- derivates (waste from forest industry). (Khan et al. 2008, 23.)

Table 1 describes compositions of some typical fuels burned in BFB boilers. All of them and biomass fuel generally have high volatile content which enables combustion in the gas phase above the bubbling bed. Ash is the mineral fraction of biomass that is left after complete combustion. Composition of fuel ashes is typically reported in either elemental percentage of weight in oxides (see Table 2) or milligrammes in kilogrammes of ash (see Table 3). Higher ash content increases particulate emission. High alkali content in ash together with silica from bed material can cause ash to melt in low temperatures. This may result in fouling of heat exchange surfaces and sintering of bed. Therefore it is important to know the composition of fuel and its ash and be aware of the possible reactions and effects. (Khan et al. 2008, 27.)

Table 1. Indicative compositions of some solid fuels used in BFB boilers.

		GROT[1]	Eucalyptus bark[2]	RDF[3]	Peat[3]
LHV	MJ/kg(db)	19.9	15.9	13–20	20.4
Moisture	%-w	35–55	53.9	15–25	40–55
Ash	%-w(d)	1–5	13.0	5–7	4–7
Volatiles	%-w(daf)	75		78–90	65–70
C	%-w(daf)	43–55	44.4	51–70	50–57
H	%-w(daf)	5–6.6	4.8	6.5–10	5–6.5
N	%-w(daf)	0.05–1.1	0.3	0.4–1.4	1–2.7
O	%-w(daf)	37–43	43.7		30–40
S	%-w(daf)	0.02–0.05	0.04	<0.1–0.2	<0.5
Cl	%-w(daf)	0.02–0.05	0.66	<0.2–1	<0.1

[1](Strömberg & Herstad Svärd 2012, 54–55) GROT is a Scandinavian forest fuel of branches and tops.
[2](Skrifvars et al. 2005, 1514.)
[3](Moilanen et al. 2002, 137.)

Table 2. Indicative composition of fuel ashes reported in oxides.

		Bark from pine wood[1]	Eucalyptus bark[2]	Peat[1]
Ash	%-w(d)	1.8	13.0	1.6
SiO_2	%-w	14.5	0.1	31.8
Al_2O_3	%-w		0.2	13.1
Fe_2O_3	%-w	3.8	0.3	11.0
CaO	%-w	40.0	52.4[a]	21.1
MgO	%-w	5.1	3.0	6.0
P_2O_5	%-w	2.7	1.5	
Na_2O	%-w	2.1	0.48	1.4
K_2O	%-w	3.4	6.0	2.0
other	%-w	28.4	36.0	13.6

[1](Skrifvars & Hupa 2002, 271)
[2](Skrifvars et al. 2005, 1514.)
[a]Rather than CaO, most of the calcium in the ash is present as $CaCO_3$.

Table 3. Properties of GROT and peat ash. (from Strömberg & Herstad Svärd 2012, 54; 316)

		GROT	Peat
Al	mg/kg(ash)	20 000	13 483
Ca	mg/kg(ash)	192 063	191 011
Fe	mg/kg(ash)	8 339	58 427
K	mg/kg(ash)	76 251	9 551
Na	mg/kg(ash)	8 573	5 618
Mg	mg/kg(ash)	20 948	14 607
P	mg/kg(ash)	17 141	6 180
Si	mg/kg(ash)	113 079	134 831

Combustion requires simultaneously fuel, adequate temperature and oxygen. Global combustion reaction in air for a fuel including carbon, hydrogen, oxygen, nitrogen and sulphur can be written as follows (Raiko 2002, 35).

$$\begin{aligned} &C_aH_bO_cN_dS_e + \left(a + \frac{b}{4} - \frac{c}{2} + e\right)(O_2 + 3.77N_2) \\ &\rightarrow aCO_2 + \frac{b}{2}H_2O + eSO_2 + \left[3.77\left(a + \frac{b}{4} - \frac{c}{2} + e\right) + \frac{d}{2}\right]N_2 \end{aligned} \tag{4}$$

Besides heat, carbon dioxide (CO_2), water vapour, sulphur and nitrogen oxides are released in reaction. Combustion of solid fuels can be divided into different stages. These stages are presented in Figure 5. First a fuel particle warms up and reaches the dehydration temperature. After the particle has dried out follows devolatilization where volatiles are released and burned when mixed with oxygen. The stage after that is char combustion. These stages of combustion can overlap when large particles are burned. The surface of a fuel particle can be on fire while the inside is still moist. (Saastamoinen 2002, 186; Mandø 2013.)

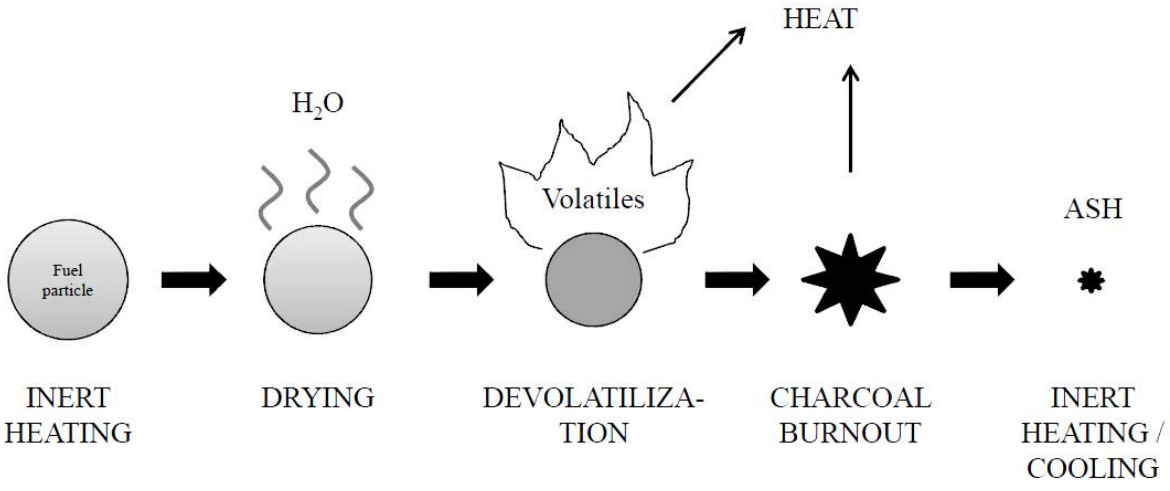

Figure 5. Stages of combustion of solid biomass fuel change as the temperature of the fuel particle rises. (modified from Mandø 2013.)

Preheated combustion air is blown to the furnace in stages to prevent incomplete combustion. Primary air is blown into the bottom of the bed through air nozzles. Primary air usually covers one-third of the combustion air. Overfire air is divided to lower and upper secondary air and tertiary air. (Hulkkonen & Kauranen 2009.) Typical need for excess air in biomass BFB boilers is 10–40 percent (Caillat & Vakkilainen 2013).

Temperature in fluidized bed and freeboard varies from 700 to 1300 °C depending on boiler design and fuel characteristics (Caillat & Vakkilainen 2013). Typical value for combustion efficiency in BFB boilers is 90–96 percent or even more. It is affected by fuel characteristics, operational and design parameters. Unburnt carbon and unburnt carbon monoxide (CO) are the two major causes of losses in combustion in BFB boilers. Unburnt carbon exits the boiler in the bottom ash and the fly ash. By growing bed and/or freeboard height, longer time for combustion can be achieved and the amount of unburnt carbon reduced. (Basu 2006, 117–121.)

2.3 Bed Area Design and Bottom Ash Handling

Furnace is where the combustion takes place. Fuel, combustion air and fresh bed material are fed into the furnace while flue gases flow from the furnace top into the second pass. Furnace has membrane walls that act as evaporator. The lower furnace walls are refractory lined to protect wall tubes from overheating and erosion. Lower furnace consists of a grid which function is to distribute fluidization air evenly through air nozzles and prevent bed material from leaking. Even distributing of air is based on adequate pressure drop over the grid. (Huhtinen et al. 2000, 157–159.) The grid consists of water tubes and plates -structure and it is not flat. It has ditches that guide removable bed material to ash hoppers and out of the bed.

Solid fuel is fed into the bubbling bed from furnace walls. Number of feeding points depends on the size of the boiler. Solid fuel is conveyed to the boiler from a day silo. Before feeding, fuel flow is balanced and shared to feeders. Furnace is equipped also with oil or gas burners to be used in start-ups.

Ash from the fuel leaves the furnace through two separate systems: bottom ash and fly ash handling. Bottom ash is collected from the bottom of the furnace. It consists of bed material and fallen slag. Fly ash consists of finer particles that have left the furnace with flue gas stream. It is collected at the bottom of second (and third) pass and at the filtration system before the flue gas stack. (Teir 2003, 95–98.) Removed bottom ash is typically handled and recycled. A classification system next to a boiler separates the coarse material

from the fine which is then returned to the furnace. The coarse matter is dumped into a container. (Huhtinen et al. 2000, 158.)

Figure 6 presents an arrangement of bottom ash handling system. Ash hoppers under the furnace grid gather the ash and guide it to bottom ash screw conveyors which are cooled with water. The conveyors move the ash to a drag chain conveyor which carries the ash towards a classification system. In this arrangement a drum sieve installed inclined works as a classification system. It consists of one or multiple rotating cylinders that have different mesh sizes. Bottom ash is fed into the drum from one end and it is sieved while moving through the drum. Fine bed material is returned to the furnace via pneumatic pipe line. Coarse refuse from the sieve is dropped to a container for later pickup.

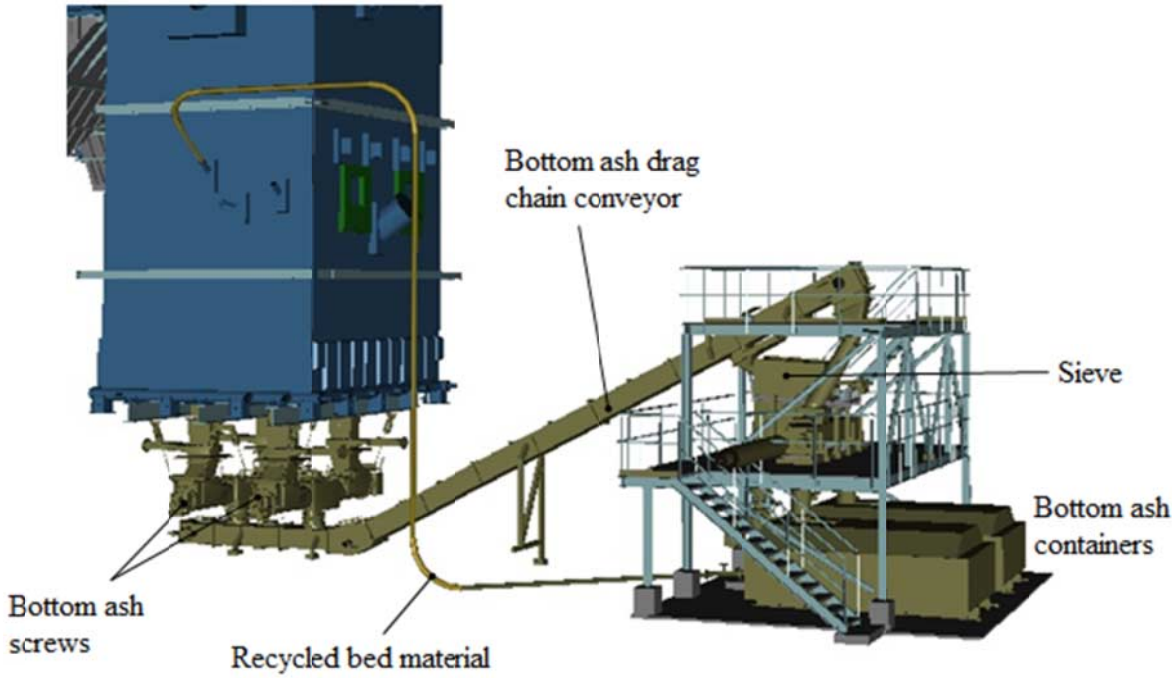

Figure 6. Layout of a bottom ash handling system consists of bottom ash screws, conveyor, sieve, refuse containers and return pipe for recycled bed material. (from Andritz Oy 2016.)

2.4 Challenges in BFB Combustion of Biomass

Biomass fuels are more reactive than fossil fuels mainly due to the high volatile content. Biomass fuels contain also alkali metals as impurities which may result in problems like bed sintering, agglomeration, slagging and fouling. And if chlorine is present, there is a

risk of corrosion as well. These ash-related problems have similar mechanisms of origin. (Basu 2003, 127.)

2.4.1 Agglomeration and Sintering

Agglomeration in fluidized bed boilers means the forming of bed material clusters. It is caused by chemical reactions and interactions between ash and bed material. (Bartels et al. 2008, 637.) These reactions and interactions happen between many different elements and compounds and are complex. Agglomeration in fluidized beds has been researched for years but is not adequately understood. (Olofsson et al. 2002, 2888)

Ashes of biomass generally contain silicon (Pi), calcium (Ca), potassium (K) and aluminium (Al). Alkali compounds tend to react with silica (SiO_2) in the bed material sand. This results in formation of alkali silicates that have low melting points (700°C). Worst possible outcome of this reaction is total bed sintering and boiler shutdown. Other factors besides the ash properties include at least bed temperature and bed material properties. (Skrifvars & Hupa 2002, 287; Bartels et al. 2008, 637.) Table 4 lists some melting points of potassium and sodium silicates. When the melting points are compared to typical temperatures of bed and freeboard, it can be noticed that the temperature circumstances can be favourable for formed silicates to melt.

Olofsson et al. (2002, 2889–2890) have observed a homogeneous and a heterogeneous type of agglomeration when different biomass fuels were burned in a pressurized fluidized bed combustor. In homogeneous agglomeration small particles grow evenly throughout the bed and fluidization is not significantly disturbed. Heterogeneous agglomeration results in larger and irregular particles that appear here and there with local temperature peaks. This causes melts that may block the whole bed.

Homogeneous agglomeration was observed when burning straw with magnesia (MgO) as bed material and clay as bed additive to bind alkalis. Respectively, heterogeneous agglomeration was observed when straw was burned with Fyle sand as bed material and calcite as bed additive. The sand used consisted of 98.2 percent of silicon dioxide (SiO_2) and was present in all of the experiments involving heavy agglomeration. These

observations done by Olofsson et al. demonstrate the importance of silicon dioxide in the case of severe agglomeration. (Olofsson et al. 2002, 2889–2890.)

Table 4. Some melting points of potassium and sodium silicates are in the area of bed temperatures. (Olofsson et al. 2002, 2893.)

Silicate	Melting point [°C]
$K_2O{\cdot}3SiO_2$	740
an eutectic of Na_2O–$CaO{\cdot}5SiO_2$ and $3Na_2O{\cdot}8SiO_2$	755
$K_2O{\cdot}4SiO_2$	764
$3Na_2O{\cdot}8SiO_2$	793
$Na_2O{\cdot}2SiO_2$	874
$K_2O{\cdot}SiO_2$	976
$K_2O{\cdot}2SiO_2$	1015
$Na_2O{\cdot}SiO_2$	1088

Abrupt temperature rises in the bed are usually required to reach the melting points of ash. Olofsson et al. (2002, 2893) state that hot spots are caused by disturbances in the bed. These disturbances include fluctuations in fuel feed and channelling of fluidization gas. Bed temperature in hot spots can reach the melting points of alkali silicates. Molten silicates stick on bed particles that may then cluster. Formed agglomerates limit the movement of other particles which may increase the local temperature further and more compounds will melt. Fluidization becomes more and more difficult and agglomeration accelerates.

When bed material is sieved and recycled to the bed, the particles undergo thermal stress that causes crackling and fragmentation. Thermal stress is caused by the repeated cooling and heating in the recycling process. Fragmented particles are coated with ash again and again. It can be assumed that significant part of the bed material is actually multi-fragment agglomerates. (Korbee et al. 2004, 32.)

Basu (2003, 128–129) lists different options to avoid agglomeration of bed:

- Use of additives like china clay, dolomite or limestone.
- Pre-processing fuels: Aim is to reduce alkali content in fuel.
- Use of alternative bed materials that react preferentially with alkali salts forming eutectic mixtures with higher melting point.

- Co-firing with coal: Sulphur in coal helps reduce the formation of agglomerates.
- Reduction of bed temperature could reduce the vaporization of alkali salts.

Some additives and alternative bed materials can be used to prevent agglomeration but these may cause new problems like blockages in air nozzles. (Mandø 2013.)

2.4.2 Slagging and Fouling

Slagging and fouling are two types of ash related problems on heat-exchange surfaces. Slagging occurs on radiant heat-exchange surfaces and fouling on convective heat-exchange surfaces. Slagging sediments are thick and have a melted outer surface. Fouling sediments have lower temperature and are mostly in solid form. (Skrifvars & Hupa 2002, 275–287.)

Ash sediments start to form when a particle reaches a heat-exchange surface and sticks on it. Particles bigger than 5 micrometres collide on the entry side of the surface and form a ridge. Smaller particles do not collide but follow the flue gas flow around the heat-exchange surface. These particles may reach the surface and stick on it by diffusion of different types. Thinner and more flat sediments are formed on heat-exchange surfaces. (Skrifvars & Hupa 2002, 275–287.)

Slagging and fouling may lead to corrosion. In the flue gas side of boiler high-temperature corrosion and low-temperature corrosion may arise. High-temperature corrosion appears on heat-exchange surfaces with high material temperatures. In practice this means superheaters. The impurities from fuels, like sulphur, potassium and sodium, tend to form ash deposits that may cause corrosion. Chloride is another impurity from fuel that can lead to corrosion. Corrosion is prevented typically by material choices depending on the designed fuel. (Caillat & Vakkilainen 2013.) Protective metal oxide layer on metallic surfaces decelerates corrosion but reducing circumstances may damage this oxide layer (Skrifvars & Hupa 2002, 284–285).

3 METHODS IN MONITORING OF BUBBLING FLUIDIZED BED

There are several ways to observe the condition of fluidized bed. Visual observation can be done from furnace sight glasses. The coarseness of bottom ash can be observed from the bottom ash conveyors. Boiler control system (DCS) gives the operator measurement data related to the bed. DCS shows the temperature profile in the bed and the pressure difference between the furnace grid and the bed. DCS also calculates the bed height. All of these methods give knowledge about the bed quality. Even so, they might not be accurate or early enough in case of agglomeration. And interpretation of observations requires experience. (Andritz Oy 2016.)

The aim in monitoring of the bed is to maintain good bed quality. But what is *good* or *good enough* bed quality? The goodness of bed conditions is a sum of many factors and always a relative subject. Some factors that can define good bed quality are:

- fluidization air flow is steady and adequate
- air/fuel ratio is suitable
- fuel feed is constant, fuel is spread well across the bed and fuel quality remains constant
- temperature profile across the bed remains steady
- bed material particle size is appropriate and uniform.

Poor bed quality causes problems in fluidization and further in steam production. Poor quality affects the hydrodynamics and could be defined as coarse particles and agglomerates that do not fluidize well or at all. These problems may result in total defluidization and boiler shutdown. Poor quality affects also combustion. Peaking of CO emissions may result from incomplete combustion.

Single generalised method for agglomeration detection and fluidized bed condition diagnostics does not exist. Literature presents several methods based on different technologies. These methods are still under development and no commercially generalized method exists.

Bartels et al. (2008, 636) classify agglomeration detection methods into on-line and ex-situ measurements (see Figure 7). Ex-situ measurement methods include fuel ash measurements and on-line measurement methods include process measurements. The most common process measurements include pressure, temperature, acoustic emissions and gas-phase alkali detection. This chapter deals with pressure and temperature measurements because these methods are most suitable for industrial fluidized beds. Acoustic emission measurement and image analysis from bottom ash are discussed in chapters 4 and 5.

Pressure and temperature are commonly measured in industrial BFB boilers. A sharp temperature gradient or pressure drop fluctuations in the bed predict the formation of agglomerates (Korbee et al., 2003). Even if pressure and temperature profiles of the bed do reflect the hydrodynamics, simple measurements solely do not help in early detection of agglomeration (Scala & Chirone 2005, 122).

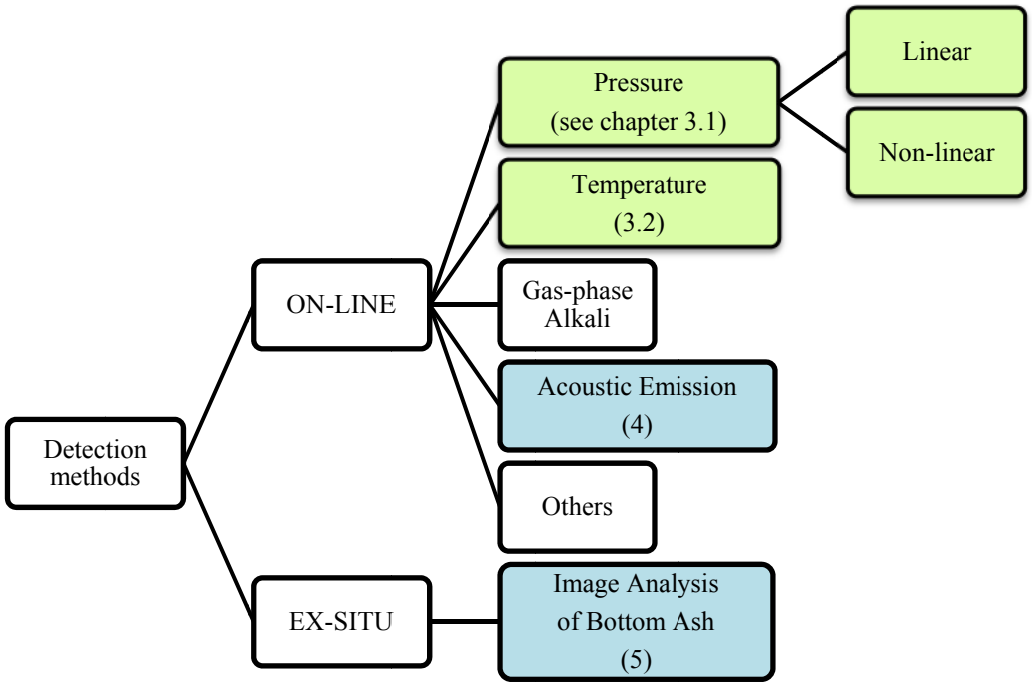

Figure 7. Detection methods are classified in ex-situ and on-line methods. Methods discussed in this chapter are coloured with green. Methods coloured with blue are discussed in their own chapters. (modified from Bartels et al. 2008, 636.)

3.1 Pressure Measurements

Pressure measurements of fluidized bed reflect its hydrodynamics and give information about the bed height and density both locally and generally. There are linear and non-linear

methods in analysing pressure measurements of bed. Linear methods include statistical methods like calculating standard deviation and variance of pressure measurement. (Bartels et al. 2008, 642–650.)

Bartels et al. (2008, 642–645) name several pressure measurement methods based on standard deviation and variance from different literature sources. Although these methods indicate sensitivity to agglomeration or increase of particle size, they all are sensitive to fluidization gas velocity. This delimits or prevents the use of these methods in industrial BFB boilers where fluctuation of superficial gas velocity is common and makes power adjustment possible. Bartels et al. (2008, 642–645) state that plain pressure measurements or simple linear methods cannot offer an early warning system against agglomeration.

Most of the non-linear pressure measurement methods are based on state-space projection of the bed. State-space representation is a mathematical model where variables governing a system are projected into a multi-dimensional space. An *attractor* is a characteristic measure of a dynamical system. It is a collection of successive states of fluidized bed at a certain time. (Bartels et al. 2008, 645–650.) Several studies about non-linear pressure measurement analysis can be found in literature. However, there is no certainty that these methods would succeed in early detection of agglomeration. Most promising method seems to be the comparison of attractors.

EARS – Early Agglomeration Recognition System

A research team from the Netherlands have developed a method to monitor agglomeration in BFB. Early Agglomeration Recognition System (EARS) uses non-linear methods to compare reference and evaluation pressure time-series. EARS was first tested on bench-scale. The tests demonstrated that EARS recognizes agglomeration 30–60 minutes earlier than it can be seen from pressure drop fluctuations or temperature differences. (Korbee et al. 2003, 1–7.)

EARS-method begins with collecting of reference time-series of pressure measurement data at the optimum fluidization state. From reference and evaluation pressure time-series attractors are produced. An attractor is "*a multi-dimensional distribution of delay vectors containing successive pressure values*" (see Figure 8a). Attractors represent fluidized bed

hydrodynamics and are like fingerprints. These attractors are compared and characteristic value S is calculated (see Figure 8b). It describes the dimensionless distance between fingerprints of reference and evaluation data. When the value of S increases, the hydrodynamics of a fluidized bed change. This increase may be an indicator of the onset of bed agglomeration. (Korbee et al. 2003, 1–7.)

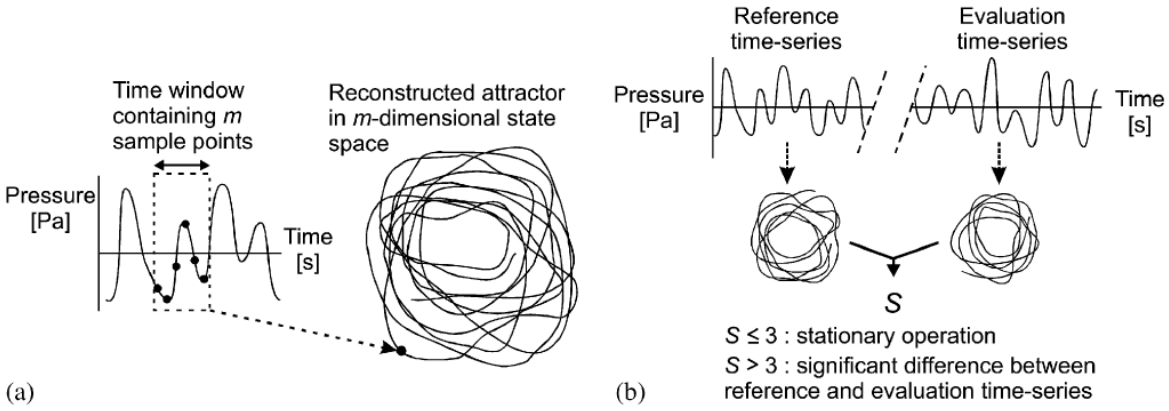

Figure 8. In EARS-method attractors are produced from pressure time-series (a) and S is calculated from attractors (b). (from Nijenhuis et al. 2007, 645)

Instead of comparing a static reference time period to a moving evaluation window, it is wise to move the reference time window in case of regularly changing operation conditions. This is called the moving reference method. Its advantage is that it rejects operation variations over a long time. But then again, the moving reference method detects a single disturbance twice. Differences between the static and the moving reference methods are illustrated in Figure 9. (Nijenhuis et al. 2007, 645.)

Korbee et al. (2003, 1–7) recommend collecting reference data for all typical operating conditions. The amount of possible conditions depends on the boiler. For example variation in fuel mixes, production demand, operating targets and methods generate different kind of pressure profiles and can vary even daily. The method tolerates some changes so that there is no need for infinite amount of reference series.

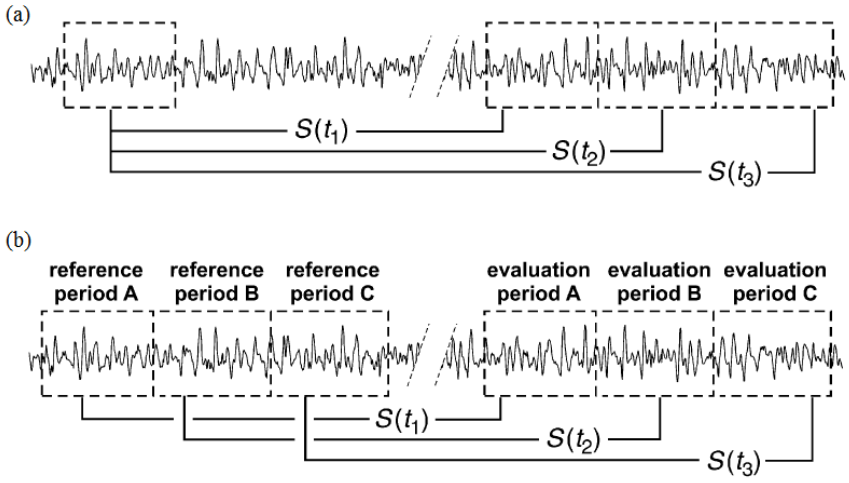

Figure 9. In static reference method an attractor is compared to attractors of reference series (a). Reference period moves with a constant time delay to evaluation period in moving reference method (b). (from Nijenhuis et al. 2007, 645.)

To reduce the sensitivity to fluctuations of superficial gas velocity pressure time series are normalized in EARS-method. This means that the standard deviation is excluded. (Ommen et al. 2000, 2186.) Insensitivity to variation of gas velocity and bed mass (height) are demonstrated. Bed mass or gas velocity changes smaller than 10 percent did not critically raise the S value. It is stated that a reference time-series should be recorded greater variations. Method is insensitive to simultaneous discharge and make-up of bed material as well. (Korbee et al. 2003, 1–7.)

Industrial prototype of EARS was installed and tested at an 80 MW_{th} BFB boiler burning wood chips. Results supported the observation made in bench-scale tests. Tests verified that the method is insensitive to 10 percent variation in process conditions. However, no agglomeration was observed during the test period. (Nijenhuis et al. 2007, 651–653.)

Nijenhuis et al. (2007, 652) propose also the possibility of filtering the S-value in order to avoid false alarms. Filtering increases the confidence level. This would be done by taking the minimum of the *n* successive S-values. Nijenhuis et al. suspect that the variation of particle size could be detected with EARS but it needs more testing in industrial scale.

3.2 Temperature Measurements

Temperature measurements in fluidized bed can be used to spot agglomeration. Local temperature differences describe the stage of mixing of the bed. When agglomeration starts, the bed becomes sticky and mixing is not as efficient as before. Therefore agglomeration can be deduced from increased temperature differences. (Bartels et al. 2008, 652–654.)

Bed temperature measurements describe the local bed mixing better than pressure measurements. However, temperatures react to changes with a delay. (Bartels et al. 2008, 652–654.) And even if changes in temperature differences can indicate agglomeration, it can result from something else too. For instance, increase of temperature differences can result from:

- the variation in fuel quality: heating value, moisture content, particle size, density
- disturbances in fuel feeding or fluidization air flow
- dropping of slagging sediments into the bed
- inoperative termoelements.

Scala & Chirone (2005, 120–132) have investigated agglomeration when combusting olive husk in a bench-scale fluidized bed. Olive husk has high tendency for agglomeration because its ash has high potassium content. Bed material used in tests was silica sand. All 14 reported runs ended up in defluidization while temperature was measured and recorded at three different heights (z) in the bed. Temperature differences were observed to increase before defluidization in every experiment.

Scala's & Chirone's (2005, 120–132) combustion experiments were carried out in steady state. Fluidization velocity remained steady and fuel feed constant through each run. On the basis of the results by Scala & Chirone (2005) it can be stated that vertical temperature difference increases and variance of single temperature measurement decreases upon defluidization as can be seen in Figure 10. Obvious changes in these graphs can be notices about 80 minutes prior to defluidization. However, results do not consider how fluctuation of fluidization velocity would affect temperature profiles. Temperature measurements do reflect the hydrodynamics of a bench-scale fluidizing bed in steady state. Monitoring of

bed conditions of an industrial-scale BFB with temperature measurements would require more tests and probably developing a mathematical model like in EARS.

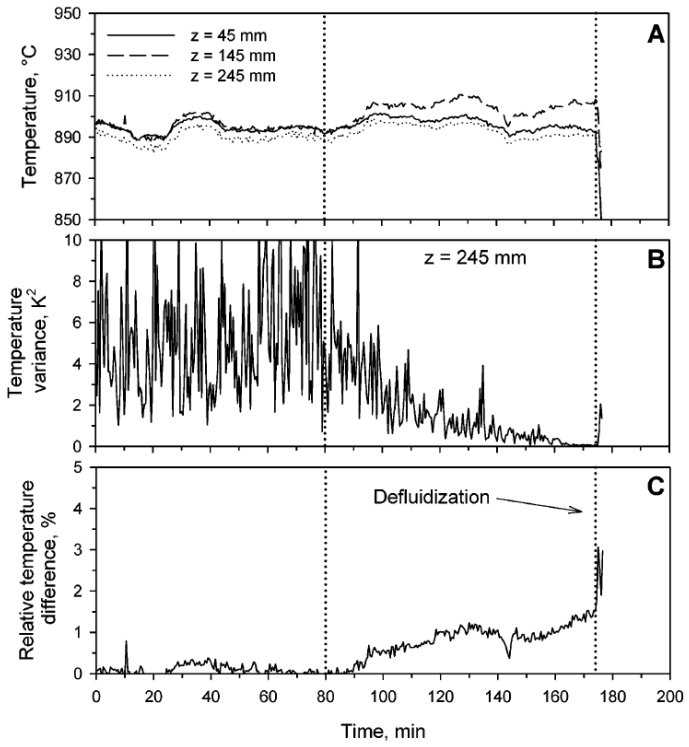

Figure 10. Temperature at three points (A), temperature variance of the highest point (B) and relative temperature difference between two lower measuring points. (from Scala & Chirone 2005, 125.)

4 ACOUSTIC EMISSION TECHNOLOGY IN MONITORING OF BED QUALITY

Acoustic emission (AE) technology is typically used in condition monitoring of both static structures and rotating apparatuses. It is used in inspection and monitoring of pressure vessels. AE data from a pressure test can indicate the weak points of structure. Constant AE measurement can reveal start of a breakdown. AE technology can also help in optimization of greasing of bearings in rotating apparatuses. (Aura 2013, 1–8.)

AE technology could have potential in monitoring the properties of a fluidized bed as well. There is recent research about utilizing AE technology in agglomeration detection in fluidized beds but not exactly in industrial BFB boilers. Most of the research is done in gas-solid fluidized bed reactors for polyethylene production. In these reactors fluidization gas velocity is generally constant. That is not the case in industrial BFB boilers. AE gives online information from the bed but is challenging to analyse. Acoustic emission sensors are low-cost and can provide online information about particle movement and hydrodynamics of fluidized bed.

4.1 Fundamentals of AE Technology

AE could be considered as an extension to the pressure measurements in higher frequencies (Bartels et al. 2008, 650–652). AE technology is based on measuring elastic high-frequency (20 kHz–1 MHz) vibration waves. The frequencies AE technology utilizes is above all other measuring methods. The vibration waves that AE is used to measure are generated, for example, by released energy upon collisions, changes in structure, deformation or breakage of material. Technology is primarily used in non-destructive testing (NDT) and condition monitoring of materials and structures. The technology can detect all events that emit elastic waves. These events include deformation, phase transition, friction, magnetic phenomena, cracking and leakage. (Aura 2013, 1–8.)

Usually piezoelectric sensors are used to convert acoustic emission into an electrical signal. Different types of piezoelectric sensor vary in sensitivity and the choice of type is case-specific (Prosser 2002, 6.2.3). The signal is amplified and filtered in analogue form

before converting it into digital signal. The digital signal can be processed further within the sampling frequency and the limits of information processing capacity of the AE unit at issue. Signal processing requires a configured integrated circuit. Data storage and a processor for data transmission should be included as well. (Aura 2013, 1–8.)

AE signals can be split to discrete and continuous signals. Discrete signals have clear beginning and end. They are produced by individual occurrences like sudden cracks and breaks in material, or collision of particles. Continuous signals are produced by continuous emission like leakage or friction. If discrete signals occur rapidly enough, they can produce continuous or near continuous emission. (Prosser 2002, 6.2.1.) Difference between discrete and continuous signal is illustrated in Figure 11.

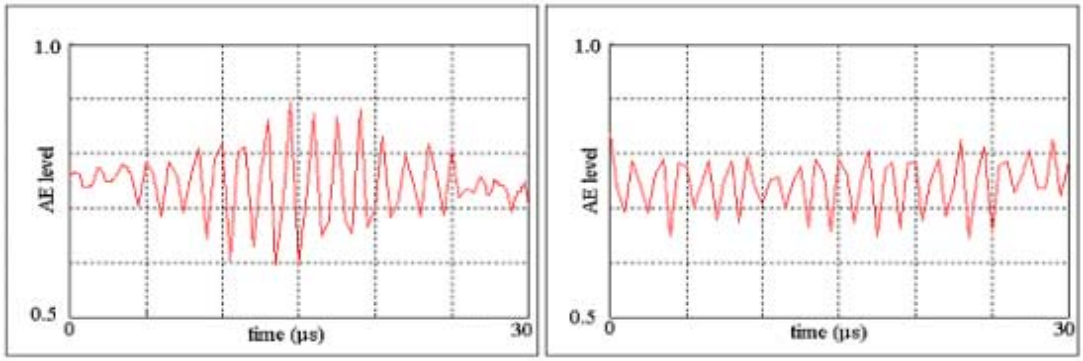

Figure 11. Discrete and continuous signals of AE. (from Salmenperä & Miettinen 2005, 2.)

Benes and Uher (2010, 1–6) have studied the use AE measuring method in determining the particle size distribution of granules of one material (clay). Experimental arrangement includes a piezoelectric AE sensor mounted at the end of a waveguide. Granules with different particle sizes were dropped and let hit on a waveguide. Arrangement is demonstrated in Figure 12. AE signals were transformed into frequency spectrums using Fast Fourier Transform (FFT).

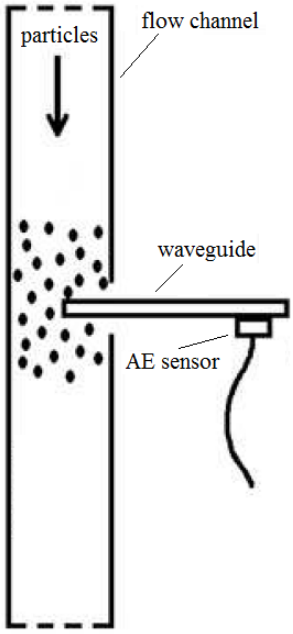

Figure 12. The principle of AE measurement of particle size distribution with a waveguide. (modified from Benes & Uher 2010, 2.)

Benes and Uher (2010, 1–6) refer to the Hertz theory of impact. They present approximations for the duration time of impact (5) and the amplitude of a force that occurs during impact (6). These equations describe the dependences AE has on particle density, velocity and radius. AE is affected also by rigidity of the particle as well as the angle of impact.

$$T \approx \rho^{0.4} v^{-0.2} r \tag{5}$$

$$F_{\max} \approx \rho^{0.6} v^{1.2} r^2 \tag{6}$$

where

T	duration of impact
$F_{\max}$	amplitude of force that occurs during impact
ρ	density of particle (mass per volume)
v	velocity of particle
r	radius of particle

Experiments by Benes and Uher (2010, 1–6) confirm what the Hertz theory implies. Smaller particles produce a frequency spectrum that has lower amplitudes at low

frequencies and higher amplitudes at high frequencies. Bigger particles produce a frequency spectrum that has higher amplitudes at low frequencies and lower amplitudes at high frequencies.

Wang et al. (2009, 3466–3473) have researched the use of AE measurements in detecting agglomeration in gas-solid fluidized bed process of polyolefin polymerization. AE sensors were installed noninvasively on the outside wall of the bed. On the basis of the research AE measurement seems sensitive to agglomeration. Wang et al. claim that it is possible to detect both moving agglomerates and wall sheeting. However, accurate arguments of detection of wall sheeting are not presented in the research. Wang et al. state that AE measurements could be utilized for agglomeration detection also in full-scale biomass fluidized beds.

AE measurements can be effective and results reliable if certain things are taken into account. Sensors should be installed symmetrically to ensure the comparability of measurement data. One has to consider sources of interference that can disturb the AE reading. This might be some electronic noise or ambient noise from operation. However, at the frequencies where AE is used there is not much noise. (Aura 2013, 1–8; Lempinen et al. 2012, 3–5.)

4.2 AE Data Analysis

The biggest challenge concerning the feasibility of AE technology is that interpretation of the collected data requires a lot of expertise starting from digital signal processing (Lempinen et al. 2012, 3–5). Plain AE signal does not usually tell much. Typical processing of AE signal includes computation of total levels, threshold values and statistical figures. (Salmenperä & Miettinen 2005, 1.) It is possible to recognize agglomeration by analysing signals with mathematical methods like standard deviation. But these methods are sensitive to changes in superficial gas flow which is usual in industrial scale fluidized bed boilers. (Wang et al. 2009, 3466–3467.)

Fourier analysis is an algorithm for integral transformation widely used in digital signal processing. Method presents a signal as a sum of sinusoidal components. Discrete Fourier Transform (DFT) is the Fourier transform for periodic digital signals and FFT is an

effective algorithm for computing DFT. The basic idea of FFT is to split the calculation into smaller DFT's. This makes the computation faster. (Turunen 2015, 52; 66–69.)

Another method for signal processing of AE is wavelet analysis. It is a time-frequency analysis method and applicable for signals with discontinuities, like AE. Wavelet transform is used for filtering of noise as well. It divides a signal into different frequency components. (Salmenperä & Miettinen 2005, 1–8; Wang et al. 2009, 3466–3473.) Many studies have applied wavelet analysis in determination of particle size distribution.

Ren et al. (2011, 260–267) have presented a model for determining particle size distribution of gas-solid fluidized bed on-line from AE. The fluidized bed reactor is used to produce polyethylene. Ren et al. describe particle size distribution model based on multi-scale wavelet analysis. Chen et al. (2008, 95–102) utilized neural networks based on wavelet analysis. Like others, Chen et al. as well leave the study of fluctuating fluidization gas velocity in the future.

Wang et al. (2009, 3466–3473) utilize chaos theory and energy fraction analysis in investigation of AE. They have developed a method in which the correlation dimension and Kolmogorov entropy (K-entropy) by least-squares method are calculated. These parameters are measures of chaos characteristics. In the research two coefficients of malfunction are produced from correlation dimension and K-entropy. In the case of agglomeration the coefficients of malfunction are much larger than that in normal fluidization.

Wang et al. determined a threshold value to indicate agglomeration. When threshold value is exceeded, the process is in malfunction which is possibly caused by agglomeration. When the process is in normal state, coefficients remain below the determined threshold value. Threshold value should be specific for each situation and conditions. However, the method cannot be referred to as an early detection method. When agglomerates have formed and are detected with AE sensors, it may be too late. Wang et al. propose the combination of AE measurement and pressure or temperature measurement to be further researched. (Wang et al. 2009, 3466–3473)

The preceding overview of AE analysis methods defends the need for a complex mathematical model for analysing AE from a BFB boiler. Concerning AE, the most challenging feature of BFB boiler is the fluctuating superficial gas flow. Wang et al. (2009, 3466–3473) consider the mathematical model of EARS (introduced in 3.1) useful and contemplate utilizing it with AE signals.

4.3 An AE Measurement System

Patent specification (FI 121557 B. 2008) for an arrangement and method for monitoring the condition of a fluidized bed describes an invention, which measures acoustic emission caused by the particles in fluidized bed and detects changes in the fluidized bed conditions. The arrangement (Figure 13) consists of a detector rod that acts as a wave guide (2 in the Figure 13) and is inserted into the fluidized bed through the furnace wall (4). Detector rod receives high frequency vibration when bed particles collide on its head. A piezoelectric sensor (7) is connected to the rod and is located outside the furnace. The sensor converts acoustic emission into an electrical signal. (FI 121557 B. 2008.)

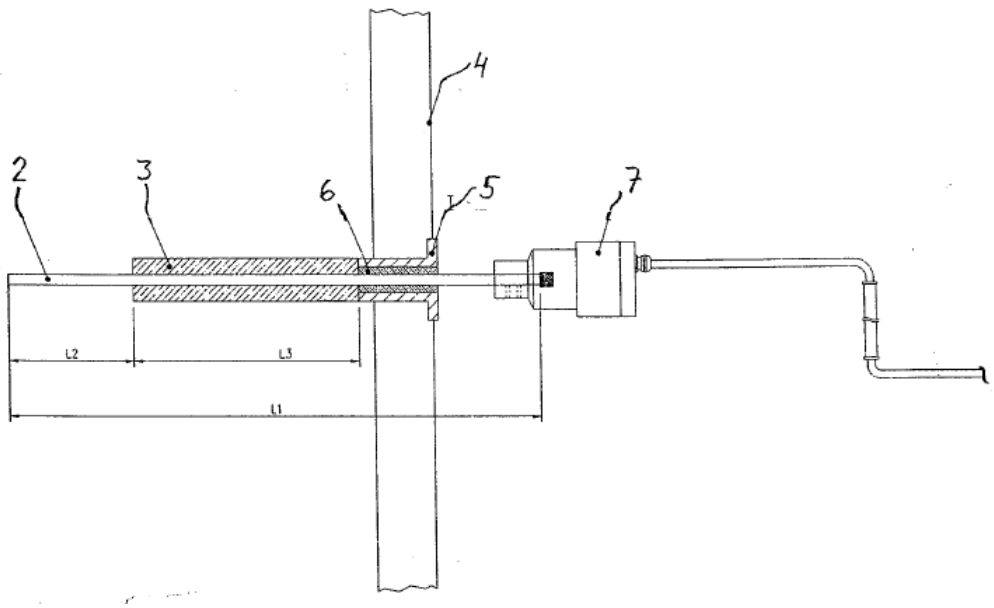

Figure 13. Detector rod is lead through the furnace wall and piezoelectric sensor is located outside the furnace. (from FI 121557 B. 2008.)

A part of the detector rod is insulated (3). The measuring area covers the uninsulated part of the rod. At the lead-in point the detector rod is covered with a bushing (5) and isolated from the vibration (6) caused by the wall. The signal is processed in an analogue filter.

Interfering frequencies are filtered out and the best frequency range is selected. The signal is then amplified and converted into digital form with an A/D converter. After filtering, digital signal is ready for data processing. Data is processed into a frequency spectrum with FFT algorithm. FFT algorithm helps to evaluate momentary state by displaying rapid changes. The patent suggests that to evaluate agglomeration a longer measurement period should be studied and an envelope graph drawn. (FI 121557 B. 2008.)

Frequency ranges used are always process and case specific. Ranges should be determined in a way that the changes in bed conditions are best represented. To get extensive information about the fluidized bed conditions, several detector units should be placed at different widths and/or heights of the bed. Acoustic emission, caused by colliding bed particles, correlates strongly to several process characteristics. Considering the risk of agglomeration the most interesting dependence is between AE and coarseness of the bed. Others include fluidization velocity, bed measurements and location of the detector. (FI 121557 B. 2008.)

5 DIGITAL IMAGE PROCESSING AS A TOOL IN MONITORING OF BED QUALITY

Analysing of bottom ash images is an ex-situ method for monitoring of BFB, particularly the size of bed material particles. Naturally, bottom ash cannot be evaluated before than it is conveyed from the boiler. This sets a delay to the analysis and that is why it cannot truly be an online system. Nevertheless image analysis system can be quite simple, easy to assemble and low-priced. There are fast developing open source software and libraries available for image analysis. Image analysis system can function independently and reliably once installed and automatic alarms are applied.

Human visual system can recognize objects extremely well but is not that accurate in measuring grey values, distances and areas. These tasks can be better performed with a digital image processing system. Even so, human intelligence is still needed to define the tasks and understand the received information. Images contain a lot of information in visual form. Image analysis is a process that aims at information extraction and understanding of images, and image processing offers the tools for it. Image processing stands for manipulation of images by computer. Image processing system requires at least the following four components:

1. A camera or a video recorder to collect images.
2. Frame grabber that converts an electrical signal into a digital image.
3. A computer where images are processed.
4. Software that offers the tools for image processing. (Jähne 2005, 3–29.)

Digital image processing enables investigation of complicated phenomena that occur in technical processes. Typical tasks to do include:

- counting particles
- determining size distribution
- retrieving 3D information from 2D image
- analysing series of images
- object recognition. (Jähne 2005, 3–29.)

Liukkonen et al. (2015, 892–897) have introduced a modelling method for fluidized bed condition based on image analysis. A system is developed and tested at an industrial scale CFB boiler. It measures the coarseness of the bed by capturing, processing and analysing digital images of bottom ash. The system calculates the sizes of bottom ash particles and represents the shares of particles of different size. In their setup a digital camera is set up above the bottom ash conveyor. When a motion sensor detects conveyor moving, the camera automatically starts to capture images.

Digital images need to be analysed to get the information on bed conditions. Liukkonen et al. (2015, 892–897) describe a computer programme developed for image analysis. It is carried out in MATLAB environment and its image processing toolbox. The programme determines the particle size distribution of ash by the following steps.

Processing begins by adjusting contrast of the greyscale image taken. The image is then converted into binary form by thresholding based on Otsu's method. After thresholding connected components in the binary image are detected. Size of the individual objects are calculated in pixels and converted to millimetres by use of the known pixel size. In the end the programme calculates areal shares of preferred and selected size classes. Images with bad quality due to moving or interfering objects, like scraper, can be eliminated by sorting recognizable image histograms. (Liukkonen et al. 2015, 892–897)

During the experimental period at a CFB boiler Liukkonen et al. (2015, 892–897) did not encounter severe coarsening or large-scale agglomeration of the bed. Bottom ash was not sieved to determine actual particle size to validate the results. But in that case particle densities should be specified too. In general the changes in bed quality are found more interesting than absolute particle sizes.

5.1 Fundamentals of Digital Imaging and Digital Image

Images can be produced from several sources including x-ray, visible and infrared spectrum. Most familiar are images based on electromagnetic radiation. Electromagnetic radiation can be imagined as photons travelling in a wavelike pattern at the speed of light. Energy of a photon is proportional to the frequency of radiation. The shorter the wavelength the more energy photons carry (see Figure 14). Other imaging types include

acoustic imaging, electron microscopy and computer imaging. (Gonzalez & Woods 2008, 7–25.)

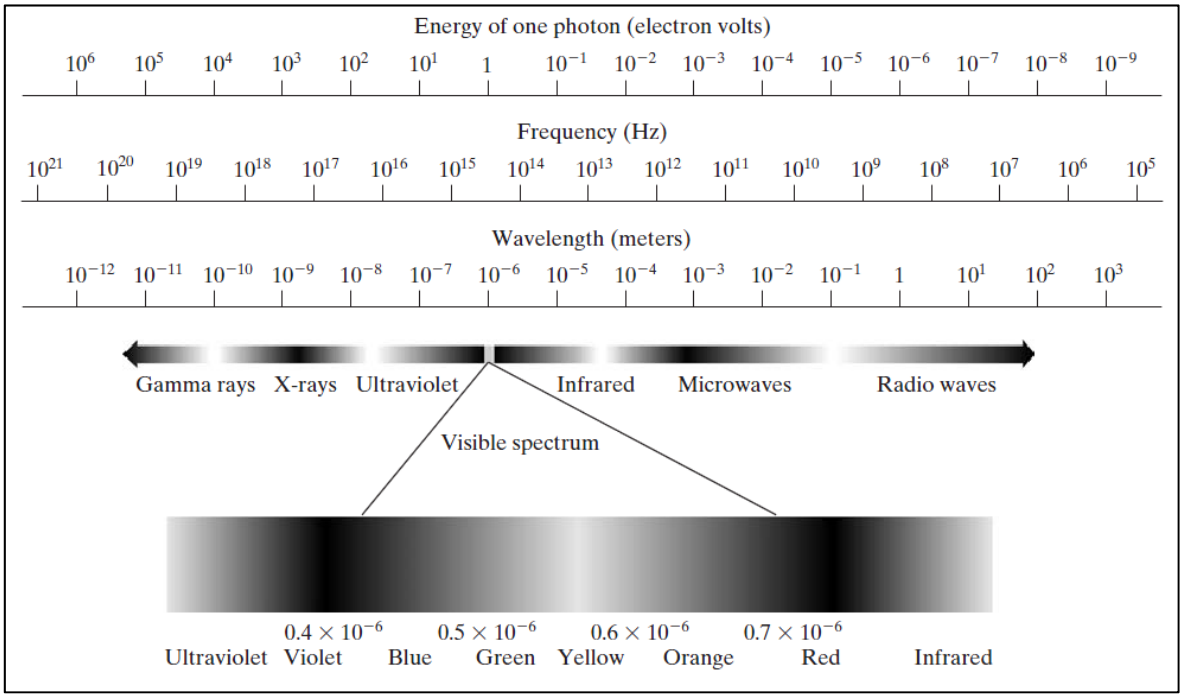

Figure 14. Electromagnetic spectrum is expressed in terms of energy, frequency and wavelength. Visible light represents a narrow portion of the spectrum. (from Gonzales & Woods 2008, 44.)

Creating a digital image starts with sensing and acquisition. Imaging sensor, shown in Figure 15, transforms incoming energy into a voltage. Acquisition can be done using a single sensor, sensor strips or sensor arrays. Generated continuous voltage waveform can be converted into digital form by digitizing both the coordinate values (sampling) and the amplitude values (quantization). (Gonzalez & Woods 2008, 46–54.)

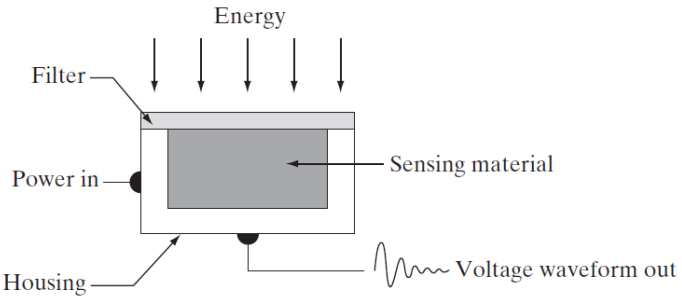

Figure 15. Single imaging sensor. (from Gonzalez & Woods 2008, 47.)

The information in a digital image can be represented in different ways. Usually spatial or wave number representation is used. The spatial representation can be converted into wave

number representation with Fourier transform. (Jähne 2005, 30–34.) Operating on an image in the spatial domain is computationally more efficient and requires less processing resources than operating in frequency domain (Gonzalez & Woods 2008, 104–107). From now on image processing is discussed only in the spatial domain while operating in frequency domain is excluded.

For a computer, an image is represented as points that form a two-dimensional array. A single point is called a pixel which is an acronym for picture element. (Jähne 2005, 30–34.) Figure 16 explains the spatial representation of an image. There are *M* rows and *N* columns that form a two dimensional array. Rows run from top to bottom and columns from left to right starting from 0. Total number of pixels, *M* x *N*, describes the resolution of an image. (Gonzalez & Woods 2008, 54–59.) An image consisting of pixels in Figure 16 can easily be represented in matrix **A** as follows:

$$\mathbf{A} = \begin{bmatrix} a_{0,0} & a_{0,1} & \cdots & a_{0,\mathrm{N}-1} \\ a_{1,0} & a_{1,1} & \cdots & a_{1,\mathrm{N}-1} \\ \vdots & \vdots & & \vdots \\ a_{\mathrm{M}-1,0} & a_{\mathrm{M}-1,1} & \cdots & a_{\mathrm{M}-1,\mathrm{N}-1} \end{bmatrix} \tag{7}$$

$$\text{where} \qquad a_{i,j} = f(x = i, y = j)$$

Monochromatic light is radiation with only one wavelength. It is colourless light but its intensity range is often called greyscale. This is because the intensity variation of monochromatic light is sensed as a sliding transition from black to white. Greyscale images are actually monochromatic images. Image analysis is traditionally performed in greyscale but full-colour image analysis might become more popular in the future. (Gonzalez & Woods 2008, 45.) However, in this study only greyscale images are discussed from now on.

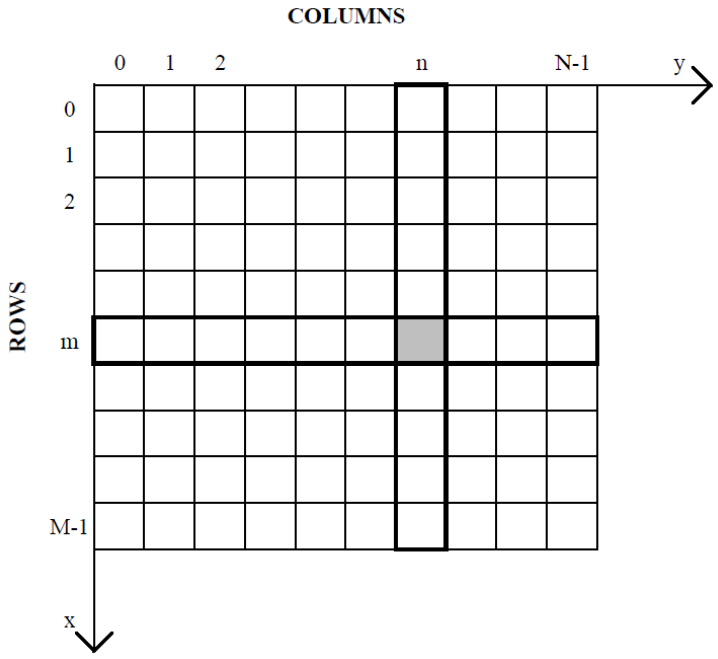

Figure 16. Digital image consists of *M* x *N* of pixels that form a *M* x *N* matrix. A pixel (*m, n*) is coloured with grey.

Histogram of a digital image portrays intensity levels and is the basis of image processing techniques. Number *L* stands for discrete intensity levels and is an integer power of 2 in the interval [0, *L*-1]. For example an 8-bit greyscale image has 2^8 or 256 levels of intensity. Typically intensity level of 0 equals black and 255 white. But this can be another way around. The levels between 0 and 255 are different shades of grey lightening from black to white. Histograms are usually portrayed in *xy*-plane so that intensity level is on *x*-axis and number of pixels is on *y*-axis. Intensity histogram can act, for example, as a tool in image segmentation. The difference between the intensity minimum and maximum is called the contrast of an image. (Gonzalez & Woods 2008, 57–58; 120.)

5.2 A Digital Image Processing Method for Bottom Ash

Basically, digital image processing is calculation with arrays or matrices. Image processing methods can be linear or non-linear. Digital image processing utilizes many mathematical operations. (Gonzalez & Woods 2008, 72–98.) Human eye can quickly acquire information about particle size from a bottom ash image. A computer could do this more efficiently especially when the amount of images gets big. Probably a computer could also find something the human eye cannot tell apart. Computer just needs to be programmed what to look for and how exactly.

In the following paragraphs an image processing method is presented and applied to an example image of bottom ash. Operations are demonstrated step by step. The objective is to detect large particles in images instead of determining the particle size distribution. These large particles may be agglomerates formed in the bed or stones from fuel feed. Open source tools used in the image processing include:

- OpenCV 3.1.0, a Python library of programming functions for computer vision
- Spyder 2.3.8, an IDE in the Python 2.7.11 language
- NumPy 1.10.1, a Python library of mathematical functions
- matplotlib 1.5.0, a Python library for plotting.

The most essential of the listed tools is OpenCV which stands for *Open Source Computer Vision Library*. It is a software library containing more than 2500 optimized algorithms for computer vision and machine learning. OpenCV is written natively in C++-language but it has also C, Python and Java interfaces. Here, the Python interface is utilized. The library is under continuous development by developers and users. Due to this, available documentation is not comprehensive yet updated constantly. (OpenCV 2016.)

5.2.1 Image Enhancement by Improving of Contrast

Original image of bottom ash used in the following example is presented in Figure 17. The image was taken at a bottom ash conveyor of a BFB boiler. It shows the surface of an ash pile moving along the conveyor. The horizontal rectangle peeking out under the ash layer is a scraper of the drag chain conveyor. The scraper's task is to move the pile of bottom ash forward on the conveyor. There is one bigger chunk near the left bottom corner of the image. It might be either a stone originating from solid fuel or an agglomerate formed in the furnace. Otherwise the bottom ash in the image seems rather homogeneous by visual examination.

Figure 17. An original colour image from bottom ash conveyor is quite dark for the human eye. Pixel resolution of the image is 1632x2464.

In the beginning of image processing the original image was converted into greyscale and resized to height of 400 pixels to boost the processing. The output image can be seen in Figure 18 with the corresponding histogram. The histogram supports the observation of a non-luminous image. Histogram has its maximum value at intensity level 25 when level 0 equals black. Next step in the image processing was equalization of histogram. The basic idea of histogram equalization is to improve the contrast by stretching the histogram. Global histogram equalization can go awry if the illumination is not even in the input image. Output of simple global histogram equalization can be seen in Figure 19.

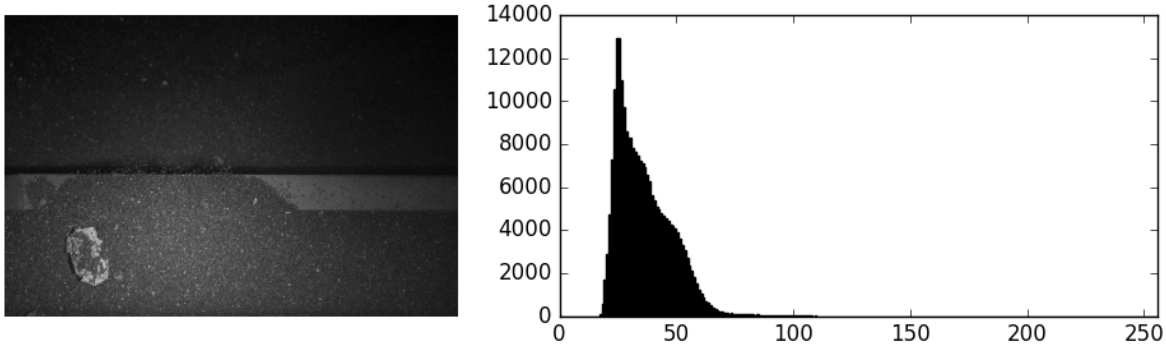

Figure 18. Original resized greyscale image and corresponding histogram. Pixel resolution of the image is 400x603.

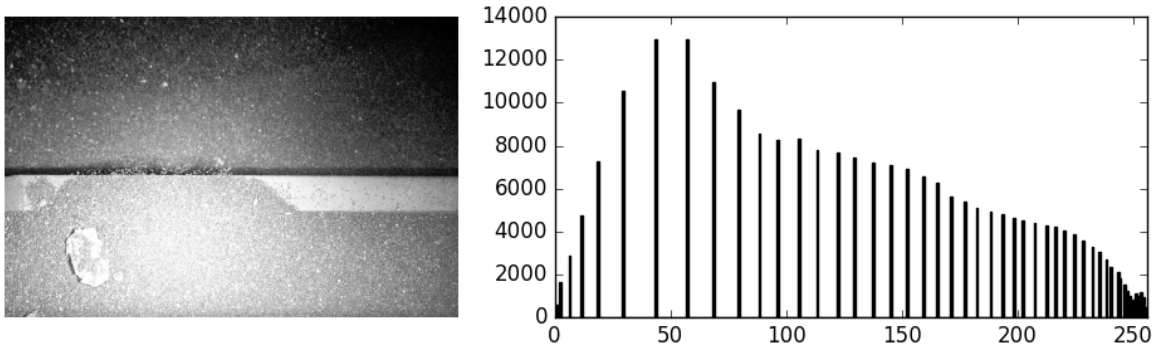

Figure 19. Output image from global histogram equalization has a stretched histogram over the intensity scale.

As a result of the global histogram equalization the most interesting part of the image has low contrast. For the image at issue, histogram equalization was better to be implemented with CLAHE-algorithm from OpenCV-library. CLAHE stands for *Contrast Limited Adaptive Histogram Equalization*. It divides the input image into small blocks called tiles. Then image histogram equalization is implemented to these tiles separately. That is how uneven illumination is taken into account. Output image after implementing CLAHE and corresponding histogram are presented in Figure 20. OpenCV-function used to create CLAHE-algorithm requires arguments as follows: (OpenCV 3.1.0 for Python 2015.)

```
cv2.createCLAHE(clipLimit, tileGridSize)
```

where clipLimit means the contrast limit
tileGridSize determines the size of a block.

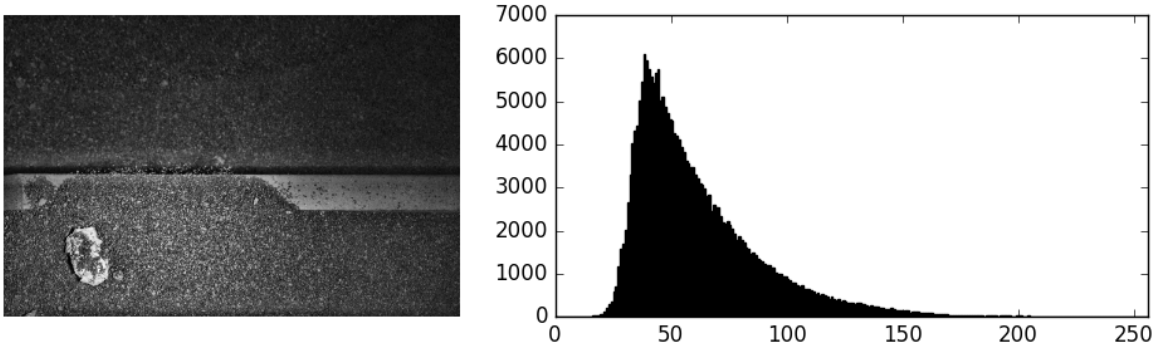

Figure 20. The image was further processed by contrast limited adaptive histogram equalization (CLAHE). Corresponding histogram is presented on the right.

5.2.2 Image Filtering

After adjusting the contrast, image can be processed on. Filtering includes operations like smoothing and sharpening an image. Filters can help to find edges in images. (Gonzalez & Woods 2008, 104–107.) Spatial filtering can be written in the following equation:

$$g(x,y) = T[f(x,y)] \tag{8}$$

where $g(x,y)$ is the output image
$f(x,y)$ is the input image
T is an operator on the input image defined over a neighbourhood of pixel (x,y).

Operator T is applied to an image with help of a neighbourhood. The centre of a neighbourhood is moved from pixel to pixel and operator T is applied to the neighbouring pixels. Output is yielded at the centre of the neighbourhood. The operator is applied to all the pixels in an image to generate output image g. At the borders, when a part of the neighbourhood resides outside of the input image, outside neighbours are simply ignored or the input image is padded with zeros. (Gonzalez & Woods 2008, 104–107.)

The shape and size of a neighbourhood determines the nature of the process. The smallest possible neighbourhood consists of the neighbourhood centre only. A neighbourhood is sometimes called a filter, a mask or a kernel. (Gonzalez & Woods 2008, 104–107.) Some common shapes of neighbourhood are illustrated in Figure 21.

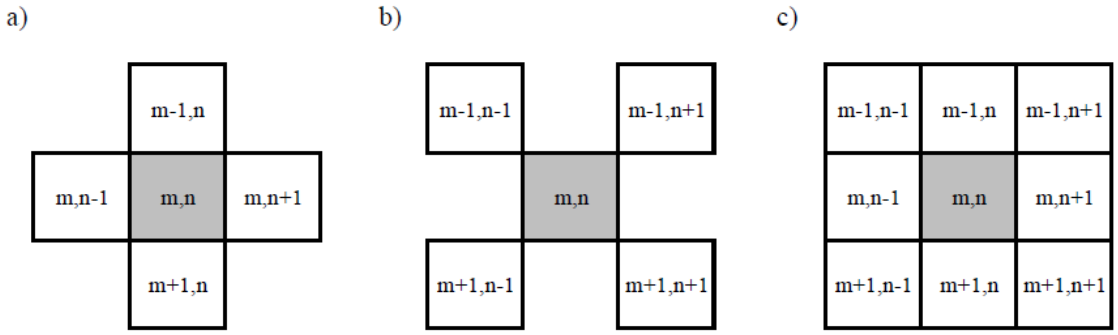

Figure 21. Example shapes of 2D-neighbourhoods: a) 4-neighbourhood b) diagonal 4-neighbourhood c) 8-neighbourhood. (modified from Jähne 2005, 34.)

There are linear and non-linear neighbourhood operations. Linear filters cannot distinguish an object feature from noise. Non-linear and adaptive filter techniques were developed to take the context into account. Object detection is an essential part of image analysis and computer vision. If individual pixels are studied and processed while neighbouring pixels are not considered, object detection is not possible. Neighbourhood operations offer tools for detection and recognition of objects and edges in images. (Jähne 2004, 315–321.)

There are several algorithms for image smoothing. Noise removal from the example image was performed with median filtering. Function used computes the median of all the pixels in the defined neighbourhood and returns the value to the centre of the neighbourhood. All the pixels of the input image are replaced with neighbourhood median in this way. Output image and corresponding histogram from median filtering are presented in Figure 22. OpenCV-function used can be defined as follows: (OpenCV 3.1.0 for Python 2015.)

```
cv2.medianBlur(src, ksize)
```

where src is the input image to be filtered
ksize determines the kernel size, ksize x ksize.

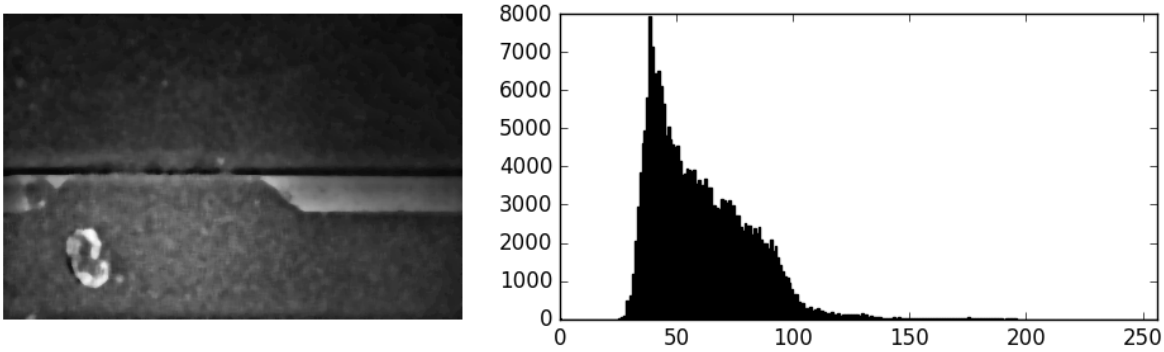

Figure 22. Median filtering reduces noise effectively. Neighbourhood size used in filtering was 9x9.

Image smoothing tends to blur also the edges of objects. If it is ideal to preserve sharp edges in objects, use of bilateral filtering should be considered. However, operation of bilateral filtering takes longer time than other smoothing operations. (OpenCV 3.1.0 for Python 2015.)

5.2.3 Image Segmentation by Thresholding

Gonzalez and Woods (2008, 689–692) define image segmentation as an image processing method where an image is subdivided into its constituent regions or objects. Level of detail used depends on the image processing problem. Special attention should be paid to segmentation accuracy. If output of segmentation is not accurate enough, computerised image analysis may fail easily. Segmentation is based on either edge or region detection. Discontinuities in intensity reveal the boundaries of regions. Sometimes it is better to detect regions with similarities instead of edges. (Gonzalez & Woods 2008, 689–692.)

One method for image segmentation is thresholding. Goal of the procedure is to separate foreground objects from background based on pixel intensity. Thresholding replaces each pixel with either black or white pixel depending on the image intensity of each pixel of input image. Therefore thresholding converts a greyscale image into a binary image. Thresholding value k can be set manually. Global thresholding function can be written in equation (9). Uneven illumination can make thresholding difficult. In that case local or adaptive thresholding functions could be used. There are several global thresholding algorithms available for different kind of images. (OpenCV 3.1.0 for Python 2015.)

$$g(x,y) = \begin{cases} L, & \text{if } f(x,y) > k \\ 0, & \text{if } f(x,y) \leq k \end{cases} \tag{9}$$

Thresholding algorithm that was used for the example image is called the triangle method. It is appropriate especially for histograms where pixels of interest produce a weak peak of intensity compared to a strong peak of background pixels. The algorithm uses normalized histogram (see Figure 23) of the input image to find the suitable thresholding value. It searches for the maximum near the histogram extremes. When the maximum is found, algorithm draws a line from the maximum to the other end of the histogram. The threshold value k is found where the distance between the line and histogram is at its maximum. The image after thresholding is presented in Figure 24. Triangle method can be utilized with an argument in thresholding function of OpenCV called `cv2.threshold`. (OpenCV 3.1.0 for Python 2015.)

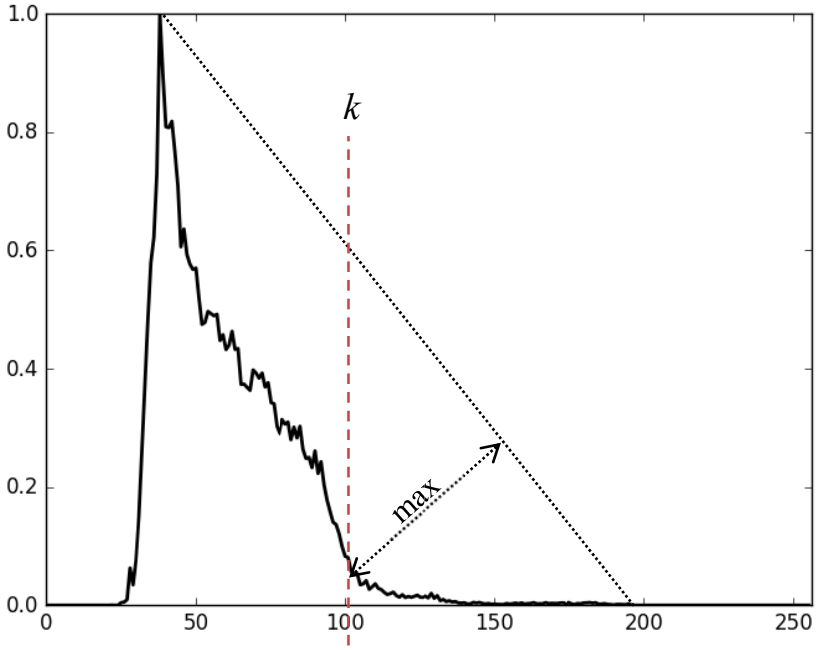

Figure 23. Idea of triangle method is demonstrated on the histogram of the smoothed image. Pixels of interest have low values of intensity compared to background pixels that form a strong peak.

Figure 24. The thresholded image includes parts of the scraper, noise, small particles and a bigger particle.

The thresholded image is processed on based on shapes to eliminate small blobs. Erosion and dilation are two mathematical morphology operations. They can be used to separate or join individual objects. Erosion eliminates irrelevant details by eroding the foreground pixels. Dilation then connects broken objects by bridging the gaps. The nature of the operation and size of the detail to be eliminated or joined is determined with a structuring element, a kernel. (Gonzalez & Woods 2002, 523–527; OpenCV 3.1.0 for Python 2015.) Functions used, `cv2.erode` and `cv2.dilate`, can be found in OpenCV-library.

5.2.4 Detecting Contours

After the image segmentation objects of interest can be identified by their shape. Functions used for contour detection are `cv2.findContours()` and `cv2.drawContours()`. Contours refer to outlines of objects. (OpenCV 3.1.0 for Python 2015.) Contours are searched with a term of minimum area. Contours smaller than defined are ignored. Found contours are sorted from biggest to smallest. Three contours found in the example image are numbered from 1 to 3 in Figure 25. When the figure is compared to original image, it is noticed that contours 1 and 3 are most probably parts of the scraper.

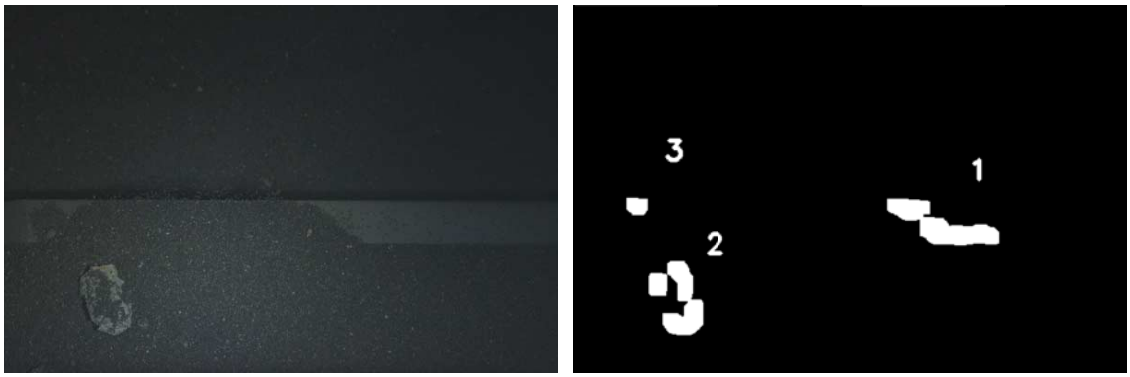

Figure 25. The programme built found three contours with area bigger than defined.

Instead of ignoring images including interfering objects and loosing information in those images, the interfering objects can be ignored. How can a computer tell particles apart from the scraper? One method could be to investigate the histograms of the contours. It can be noticed from the original image that the scraper has lower contrast than bed particles. When the normalized histograms of found contours are investigated (see Figure 26), it can be noticed that contours portraying parts of the scraper have a clear single peak. This is because the colour of scraper consists of few shades. Contours portraying stones or agglomerates have wider histograms instead of single peaks because bigger particles have many shades of colour. From the shape of the histograms it can be concluded that the histogram medians differ. Medians of scraper histograms are much smaller than medians of histograms representing stones or agglomerates. Medians of histograms are calculated with Numpy-function `np.median()`.

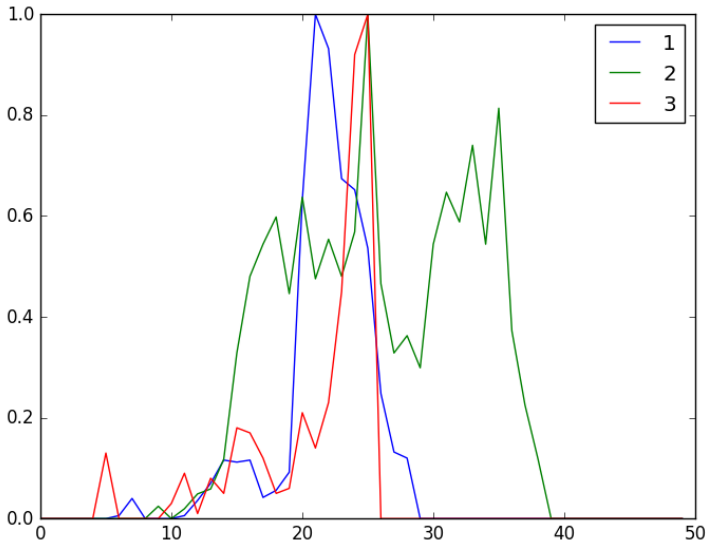

Figure 26. Normalized histograms of the found contours are distinguishable from each other. In this example the medians of histograms 1 and 3 are equal to 0.00 and the median of histogram 2 is 0.08.

By defining minimum value for the area of the contours found and a maximum for the median of the normalized histogram, only desired contours can be drawn. Image processing and analysis could continue from here to determination of the size of the particle found. That is possible when the pixel size (pixel/mm) is known. An alarm can be set for particles of interest.

6 REDUCING SAND CONSUMPTION AT A BFB BOILER

The empirical study covers a test period at a BFB boiler. It produces steam primarily for a forest industry process but also for power production and district heat. The boiler at issue has a fuel input of about 90 MW. Fuel used is a mix of forest residues, bark, peat and sludge from forest industry. Composition of the fuel is presented in Table 5. Bed material used is natural screened sand with particle size not more than 2 millimetres. The majority of sand particles are between 0.5 and 1.0 mm. Duration of the test period was 80 hours. During the test period a sample of fuel and samples of bottom ash were collected. Some process data was collected also before and after the actual test period in order to get reference data.

Table 5. Analysis of the fuel mix burned in an industrial BFB boiler.

		Fuel mix
LHV	MJ/kg(daf)	19.25
Ash	m-%	4.1
Volatiles	m-%	75.3
C	m-%	51.7
H	m-%	6.3
N	m-%	0.62
Cl	m-%	0.013
S	m-%	0.067

The objective of the test period was to reduce the consumption of fresh bed material by increasing bed material recycling. At the same time it was crucial to observe process data and quality of bottom ash to get information about the bed conditions in order to avoid any disturbances. Another objective of the test period was to estimate the feasibility of two novel systems in observation of bed conditions. This was carried out by collecting data from the bottom ash images and AE measurements for later investigation of the data. The camera system and AE sensors have been installed at the boiler some time ago but not exploited.

The risk in increasing the bed material recycling is that the alkalis accumulate in bed. To secure steam production it was important to avoid problems in fluidization. That is why changes made to the settings had to be cautious. No limiting values were searched.

Samples and some process data were analysed to get information about the bed quality. The main assumptions and simplifications made in the following inspection were:

- fuel mix and its content are considered constant
- bed height and volume are considered constant
- densities of fresh sand, bed material and bottom ash are considered the same (1500 kg/m^3).

6.1 Description of the Bottom Ash System

Figure 27 presents a simple flow chart of the bottom ash handling and recycling at the boiler at issue. The systems studied, bottom ash camera and acoustic emission measurements, are marked with red.

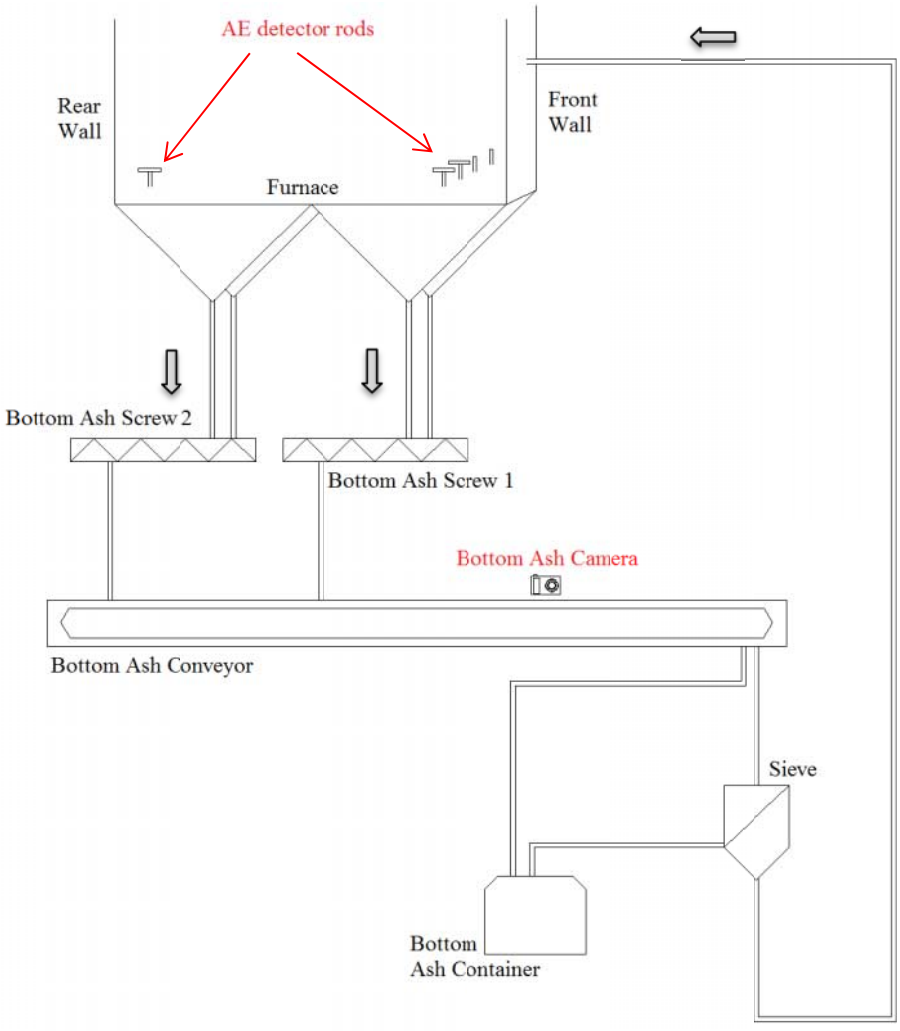

Figure 27. Bottom ash is removed from the furnace bottom and conveyed to the sieve for recycling. Acoustic emission detectors are installed in the bed and bottom ash camera at the bottom ash conveyor.

A bottom ash sequence starts when the bottom ash screw 1 starts to run and discharges bottom ash from the front wall side ash chutes to the screw. When screw 1 has run the time set, screw 2 starts to run and bottom ash from the rear wall side is discharged. Simultaneously drag chain conveyors convey the bottom ash towards a drum sieve. The sieve screens the bottom ash. Particles smaller than 1.5 x 1.5 mm are returned back to the furnace via pneumatic tube line. Reject from the sieve is conveyed to a container to be collected later. Once in every *X* times the sieve is by-passed and bottom ash is dumped straight to the container. This is done to prevent the harmful enrichment of alkalis in bed material. Dumped bed material is compensated with feeding of fresh sand from above the bed.

In practice it is known that the significant majority of bottom ash removed from the bed is returned to the furnace. In the long run the amount of reject from the sieve can be considered negligible when compared to the amount of dump that has by-passed the sieve. So in the following inspection it is assumed that total rejected bed material mass equals the mass of reject from the sieve by-pass.

6.2 Changes Made to the System Settings

The following describes the course of the test period step by step. Changes were made to the bottom ash system and sand feed system settings. Duration of the bottom ash sequence is determined by the running time of the bottom ash screws, waiting time before their restart and delay time. Initial settings (t=0) and changes made during the test period are presented in Table 6. In the beginning the bed is assumed to be in a balance state.

Table 6. Initial settings of bottom ash system were modified at given times.

at time t	[h]	0	6	10	32	50	56
BOTTOM ASH SYSTEM							
Sequence starting interval	[min]	15	"	"	"	"	"
Bottom ash screw 1 running time	[s]	80	"	"	100	"	"
Bottom ash screw 2 running time	[s]	70	"	"	50	"	"
Sequences the sieve is in use	[-]	10	13	"	"	"	15
Sequences the sieve is by-passed	[-]	1	"	"	"	"	"
SAND FEEDING							
Sand screw run time	[s]	30	"	"	"	manual	"
Sand screw pause time	[min]	40	"	44	"	manual	48

First modification, at time *t*=6 hours, was the increase of bottom ash recycling by increasing sequential times to use the sieve from 10 to 13. With this change every 14th removal from the furnace bottom was dumped without sieving and recycling. At time *t*=10 hours, feeding of fresh sand into the furnace was reduced by raising the waiting time between the sand screw runs from 40 to 44 minutes. Purpose of this action was to keep the bed height constant. When less bed material is removed from the furnace, less compensating material should be fed in.

Before and after the first modifications had been made, the quality of bottom ash was visually observed at the bottom ash conveyor. Distinct difference in coarseness between the removal from the front wall side (screw 1) and the rear wall side (screw 2) was detected. Removal from the front wall side seemed to be coarser than from the rear wall side. This difference can be seen in Figure 28. Bottom ash from the front wall side included more stones. Because of this observation done, it was decided that to attain more balanced bed, removal from the front wall side should be increased. Therefore the share of the removal from screw 1 was increased from 53 to 67 percent (80 s → 100 s). The total time of bottom ash screws running was kept at 150 seconds. This stands for 15 tons of bed material removed from the bed every day, the most of which is recycled and returned to the bed.

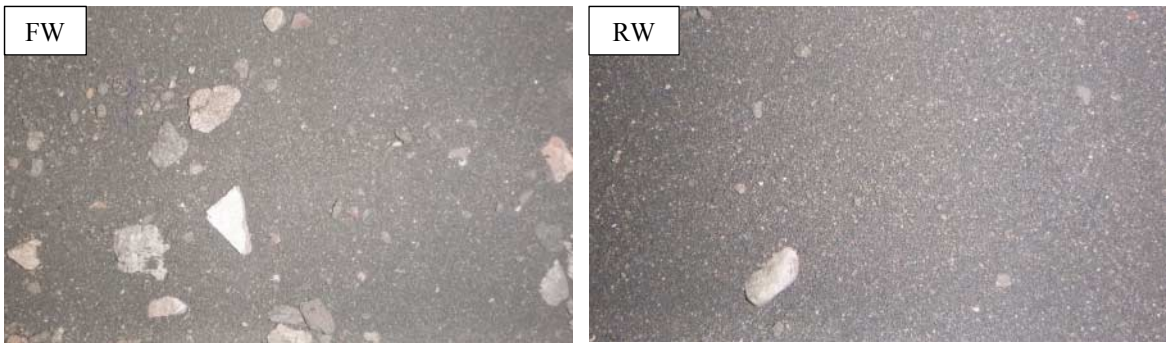

Figure 28. Bottom ash samples were photographed at t = 32 h. The sample from the front wall on the left and the sample from rear wall on the right.

At time *t*=50 hours, the calculated bed height showed decreasing and the sand screw was driven manually for a moment. The decrease seemed to be the consequence of a leak at the return tube line in bed material recycling. At this point the quality of bottom ash was

observed visually from the conveyor and it seemed to be really good. The difference between the front and rear wall sides appeared to have diminished.

Figure 29 represents linear trends of the average bed temperatures during the test period. There are 9 temperature measurements evenly installed in the bed. These measurements are generated into three average temperatures on front wall, central and rear wall sides. It can be seen that the bed temperatures drew slightly nearer each other as the test went on. Especially average temperatures on the rear wall side show increasing. That is, the temperature difference between the front and the rear of the bed decreases. This probably results from the change made to the balance between running times of bottom ash screws. The development of bed temperatures may indicate an improvement in mixing of the bed. It supports the visual observation that the change made evened out the quality of bed material.

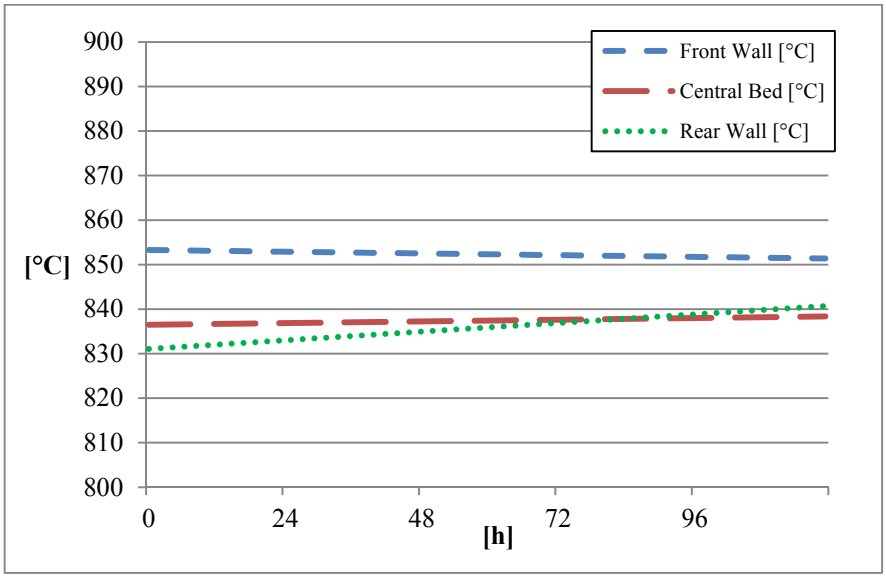

Figure 29. Linear trends of average bed temperatures show how bed temperatures drew nearer each other over 5 days from the start of the test period.

The last modification to the settings was done at time *t*=56 hours. The sequential times to use the sieve were increased from 13 to 15. From that point on every 16th removal from the furnace bottom was dumped without sieving and recycling. Table 7 shows the effect the adjusting of sieve settings has on the theoretical volume of dump. The volume of dump can be used to estimate the consumption of fresh bed material. The dumped bed material needs to be made up with fresh sand. In the long run, the mass of bottom ash dumped without

sieving is equivalent to the mass of fresh sand fed into the furnace. In practice, these are not the only solid particle flows to and from the bed. Ash from the fuel becomes bed material and some of the ash and sand escape from the furnace with flue gases. Also stones and other incombustible matter enter the boiler with fuel and exits with bottom ash.

Table 7. Sieve operating settings have essential influence on volume of dumped bottom ash.

		t=0	*t*=6	*t*=56
Sequences sieve is in use	[-]	**10**/11	**13**/14	**15**/16
Sequences sieve is by-passed	[-]	1/11	1/14	1/16
Direct dump	[%]	9.1	7.1	6.3
Direct dumps per day on average	[1/d]	7.2	5.7	5.0
Direct dumps per day on average	[t/d]	1.35	1.06	0.93
Decrease of direct dump	[m-%]		**-21 %**	**-31 %**

The theoretical capacity of a bottom ash removal sequence can be calculated using the screw capacities and bottom ash sequence parameters. In practice the volume of removal might not be constant. In theory, the changes made would decrease the volume of direct dump theoretically by 31 percent from the initial setting. This seems a little shaky estimation for sand consumption because of the volumes calculated. About a ton per day is much less than assumed by boiler staff.

Another way to estimate the sand consumption is by way of sand load information. Average sand consumption according to incoming sand loads had previously been 2.2 tons per day over a period of 6 months. Latest sand load arrived on the first day of the test period and sand silo was filled. Subsequent filling took place 35 days later. If sand consumption was calculated from incoming sand loads, for the period during and after the tests consumption would be 1.3 tons per day. Hence, sand consumption was reduced by 0.9 tons per day. That is reduction of 42 percent. This estimation does not take into account that boiler operating mode has varied according to the executed production plan. Consideration of only one load is not very trustworthy because loads vary a little.

Third way to estimate the sand consumption is calculating the theoretical consumption with the help of sand feed settings. Screw run time was kept at 30 seconds while pause time was adjusted. The affect adjusting the pause time had can be seen in Table 8. Sand

feeding was reduced 16 percent from initial settings. This estimation does not take into account that sand screw is occasionally operated manually.

Table 8. Adjusting the pause time of sand screw affects the sand consumption.

		t=0	*t*=10	*t*=56
Screw run time	[s]	30	30	30
Screw pause time	[min]	40	44	48
Sand feed	[t/d]	1.11	1.01	0.93
Decrease of sand feed	[m-%]		**-9 %**	**-16 %**

The consumption reduction can be considered to be something around these three approximations as presented above. The most credible is the approximation from sand screw run times. It is known that at ton of sand costs about 27 euros. For example, a 3 tons consumption per day would result in annual sand cost of about 30 000 euros. 16 percent decrease in sand consumption in that case would save about 5 000 euros per year.

6.3 Particle Size and Composition of Bottom Ash

Six samples of bottom ash were collected from the bottom ash conveyor. The conveyor was stopped twice during a sampling sequence. First samples came from the front wall side and second samples from the rear wall side. Even when the ash from separate screws is discharged to the same conveyor, there is noticeable gap between the batches. Samples were collected straight from the conveyor with help of an instrument and bagged for later sieving and analysis. Sample sizes varied from 1 663 to 2 080 grams. The samples were sieved by hand with 0.5 and 1.0 millimetres sieves. Figures 30 and 31 represent the determined particle size distribution by weight of samples from the front and rear wall screws.

From the sieving results can be noticed the coarseness difference between front wall and rear wall sides in the beginning of the test period. Bottom ash was coarser on the front wall side than on the rear wall side as it was visually observed. At time *t*=32 hours 75 percentage by weight of the front wall sample had particle diameter smaller than 1.0 millimetres. For the rear wall sample the percentage was 83. As the tests went on the share of particles smaller than 1.0 mm was increased on the front wall side.

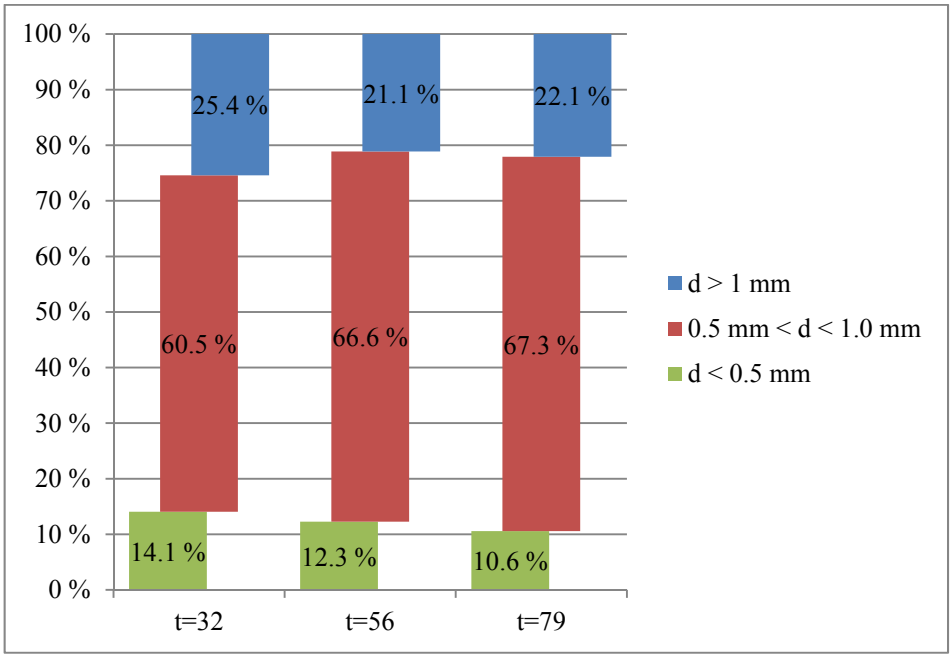

Figure 30. Bottom ash samples from the front wall side were sieved by hand and the particle size distribution was determined by weight. Over 60 percent of the particles have diameter between 0.5 and 1.0 millimetres.

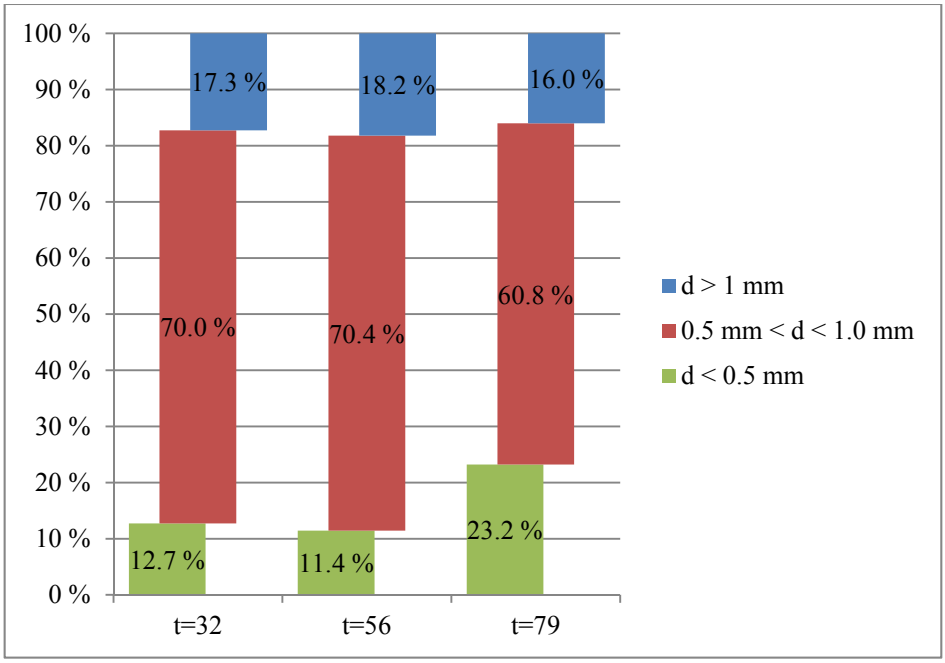

Figure 31. Bottom ash samples from the rear wall side were sieved by hand and the particle size distribution was determined by weight. About 70 percent of the particles have diameter between 0.5 and 1.0 millimetres.

As the tests went on, the share of particles with diameter less than 0.5 millimetres decreased. The rear wall sample at time *t*=79 hours differed exceptionally from the development of particle size distribution. Sample was finer than any other sample. This is likely because collecting of the sample failed at first try and it needed to be retaken.

Collecting procedure differed from other samples. Distribution of the sample at issue should be ignored. Photos taken of the samples are shown in Figure 32.

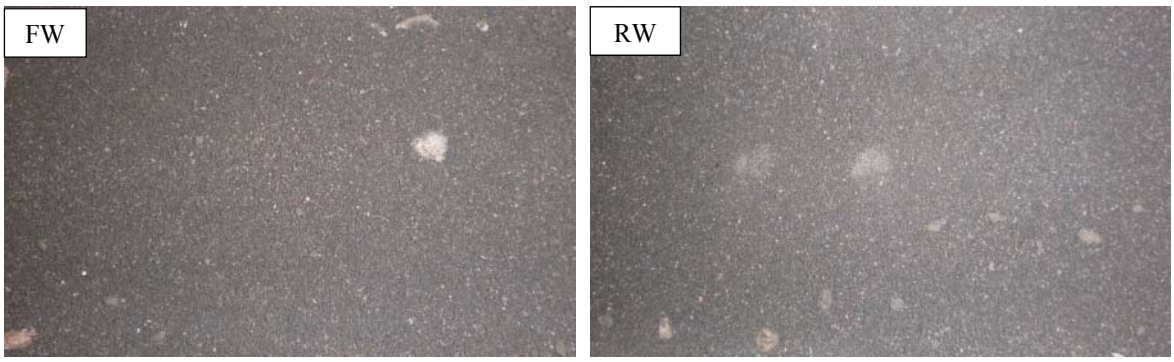

Figure 32. Bottom ash samples photographed at t = 79 h show that the quality is more balanced than in the beginning. The sample from the front wall on the left and the sample from rear wall on the right.

Four bottom ash samples were analysed in detail for metal contents too. Calcium, potassium, sodium and magnesium contents in the ash samples were determined at times t=32 and t=79 hours. Figure 33 and Table 9 demonstrates how metal contents of bottom ash developed during the tests.

Table 9. Percentage increase/decrease of metal contents in samples (t=79) of bottom ash relative to the first sample.

	Front wall samples	Rear wall samples
Al	+ 15.7 %	+ 1.8 %
P	+ 30.8 %	+ 15.4 %
K	+ 25.0 %	+ 8.6 %
Ca	+ 19.5 %	+ 9.3 %
Mg	+ 21.7 %	+ 9.4 %
Na	+ 12.5 %	+ 0.0 %
Si	0.0 %	- 5.6 %
Fe	0.0 %	+ 16.7 %
Ti	+ 19.2 %	+ 13.4 %

According to the results, alkali and earth alkali contents increased following the changes made. Of alkalis analysed, phosphor and potassium contents increased percentually the most. At time t=32 hours bottom ash samples from the rear wall side had higher metal contents than the samples from the front wall side. This indicates that as for alkalis, the replacement of bed material was more efficient on the front wall side than on the rear wall side of the furnace. At time t=79 hours alkali contents of the bottom ash from the front wall

side had increased more than of the rear wall side. This might be because the solid fuel is fed into the bed from the front wall. Increase of alkali contents is the consequence of reducing the amount of dump. The differences between front wall and rear wall side are probably due to that the mixing of the bed might not be perfect. Even if the alkali contents increased, no disturbances in the process were detected. On the grounds of only two samples per screw no firm conclusion about alkali balance can be drawn. However the results can be considered approximate.

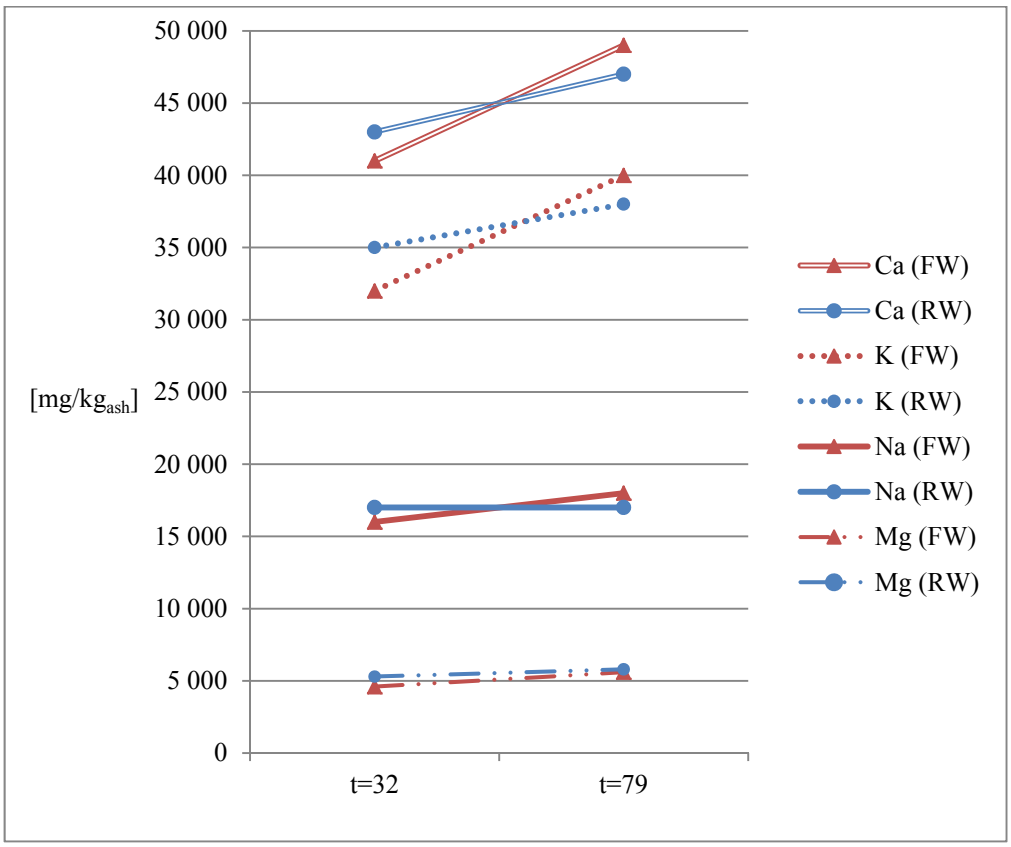

Figure 33. Ash samples were analysed at *t*=39 and *t*=79 for calcium, potassium, sodium and magnesium contents as mg/kg of ash. Front wall samples are marked with red triangles, rear wall samples with blue circles.

6.4 Study of the Data from Bottom Ash Camera and AE System in BFB

The following presents pieces of data collected from the bottom ash camera system and the AE system and examines it. The accuracy of the information drawn is evaluated.

6.4.1 Data from Image Analysis of Bottom Ash

The bottom ash camera is installed at the drag chain conveyor. System detects the conveyor moving and takes images. Images are stored on a computer connected to the camera system. Some of the images taken were discarded because of poor quality resulting from dust. The rest were analysed in MATLAB environment by a subcontractor in the way described in chapter 5. The system was not online at the time of the test period and the analysis was done with a delay. In total 560 images were analysed over a 9-day period including the test period. The results from the analysis present the areal shares of particles with diameter less than 0.5, 1.0 and 1.5 millimetres.

Figure 34 shows the share of particles of different size according to the results from image analysis. Decreasing of actual shares would tell about coarsening of the bed. It can be seen from the figure that the density of images analysed in the beginning of the test period is lower than on average. If only the time frame of the test period is viewed, a clear decreasing of the share of particles smaller than 1.5 millimetres can be noticed. When the time frame is extended to cover 68 hours before and 79 hours after the test period, supposed decreasing of shares is not that clear. As it can be seen in the Figure 34 only about 50 percent of particles have diameter smaller than 1.5 mm.

Table 10 describes the average shares of different size particles over time before, during and after the test period. Before the test period on average 41.2 percent of the particles were smaller than 1.5 millimetres. After the test period the share has slightly decreased to 39.5 percent. Shares of particles smaller than 1.0 and 0.5 millimetres show slight decreases as well.

Table 10. Average particle size distributions before, during and after the test period according to the bottom ash camera system.

	Images analysed [-]	Time frame [h]	d < 0.5 mm [%]	d < 1.0 mm [%]	d < 1.5 mm [%]
Before	133	68	3.7	21.9	41.2
During test period	155	80	3.6	21.3	40.1
After	273	79	3.8	21.4	39.5

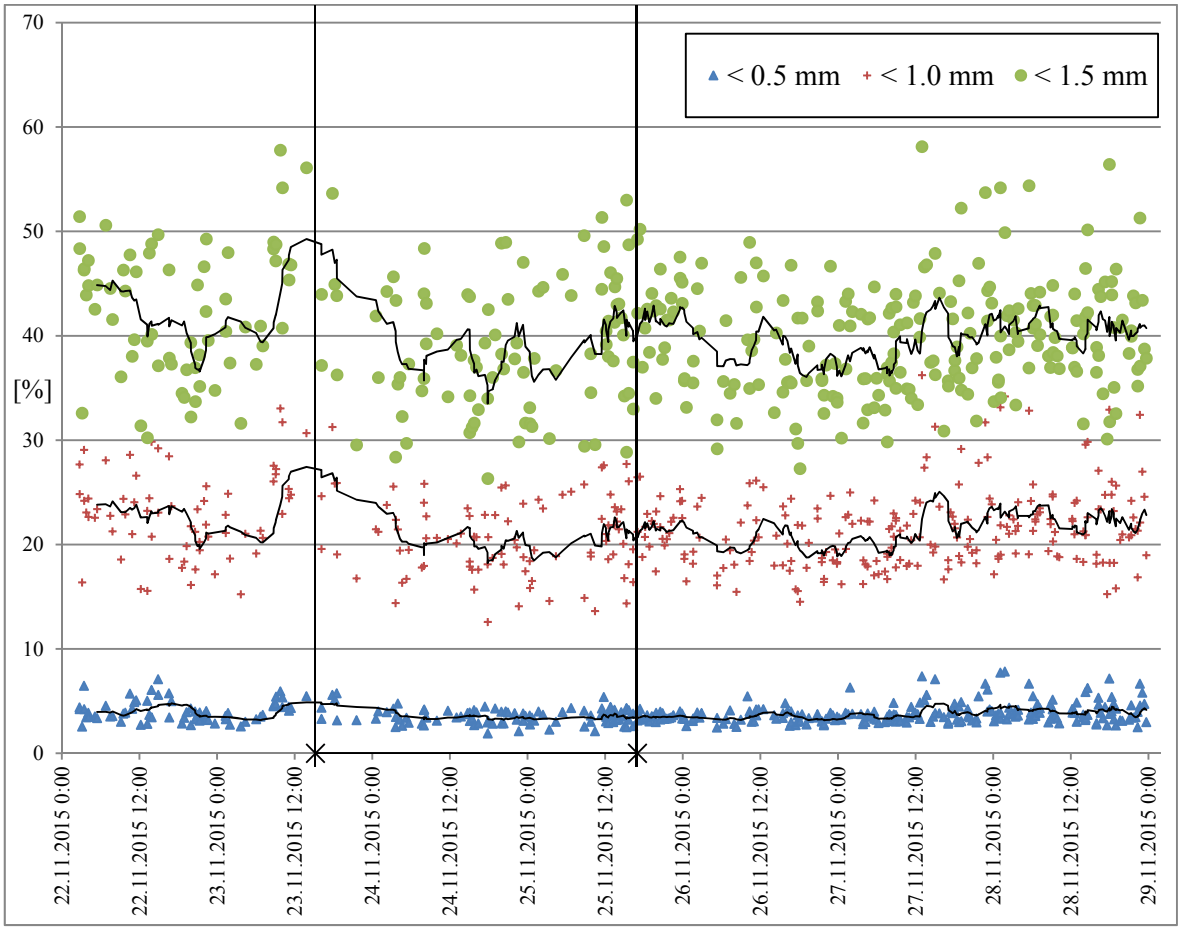

Figure 34. According to the results from image analysis of bottom ash images about 50 percent of particles have diameter smaller than 1.5 mm. Vertical lines show the moment of the first and the last modification done. Curves are moving averages of 10 consecutive images.

When the results from the bottom ash camera system are compared to the particle size distribution of collected bottom ash samples (see Figures 30 and 31), it is discovered that the results from image analysis do not correspond to the result from manual sieving. Sieving results tell that more than 60 percent of the bottom ash particles have diameter smaller than 1.0 mm. This difference might be due to that the coarser fraction of the ash moves on top of the pile while fine fraction sinks between bigger particles. This would result from bigger particles being better represented than smaller particles in an image.

6.4.2 Acoustic Emission Data from the Bubbling Bed

AE measurement system consists of five piezoelectric sensors under the furnace of the BFB boiler. The sensors are connected to five waveguides that stand between air nozzles in the bed. Two of these waveguides are installed vertically (A, B) and three horizontally (C,

D, E) (see Figure 35). Horizontal waveguides are T-shaped. Measuring area consists of the uninsulated part of the rod. The stem is 100 mm high starting from the air nozzle level and the head is 210 mm long. Vertical waveguides are 100 mm long starting from the air nozzle level. Hence, the waveguides C, D, and E have more surface area than A and B for particles to collide with. The rough location of these detection rods is demonstrated in Figure 36. As can be seen in the figure, rods A, B, C and D are installed near the front wall of the boiler and E is near the rear wall. Inner rods on the front wall side are in the area where solid fuel hits the bed.

Each piezoelectric sensor sends continuous signal to ACD-sensor. It calculates continuous FFT which is then split to frequency bands. Five frequency bands of interest have been chosen earlier to monitor. Each of these bands has the same width. Every second the sensor sends minimum, maximum and average values of intensity level on each band onto an AE server. In this study only average values are investigated.

Figure 35. The waveguides are installed between the air nozzles. On the left a rod is positioned vertically and on the right a rod horizontally.

AE data from the sensors is saved on the server that can be accessed on a Linux-computer at the boiler or remotely. A Java-based ACD Optimatic-programme with its trend tool enables user to examine the FFT of each sensor and each frequency band together with process data (e.g. bed temperatures, pressure). Programme also enables user to generate further calculations in the form of soft sensors. Frequency bands are here numbered from 1 to 5, from the lowest to the highest frequency band. The bands have the same width.

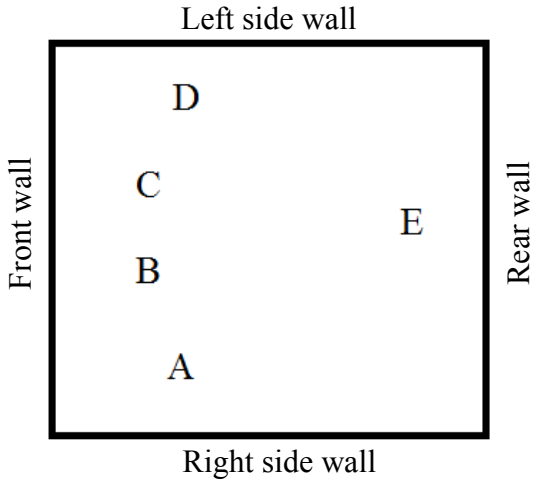

Figure 36. A rough layout of wavequide locations in the furnace profile.

Example views of AE data in the user interface are presented in the following figures. Figures 37 and 38 present the average intensity values from frequency bands 2 and 5 of sensor E on the rear wall side of the furnace together with the fluidization velocity. Figure 39 presents the subtraction of these two values (2-5). Time period of these trends is 21 days including a week before the test period, the week of the test period and a week after it.

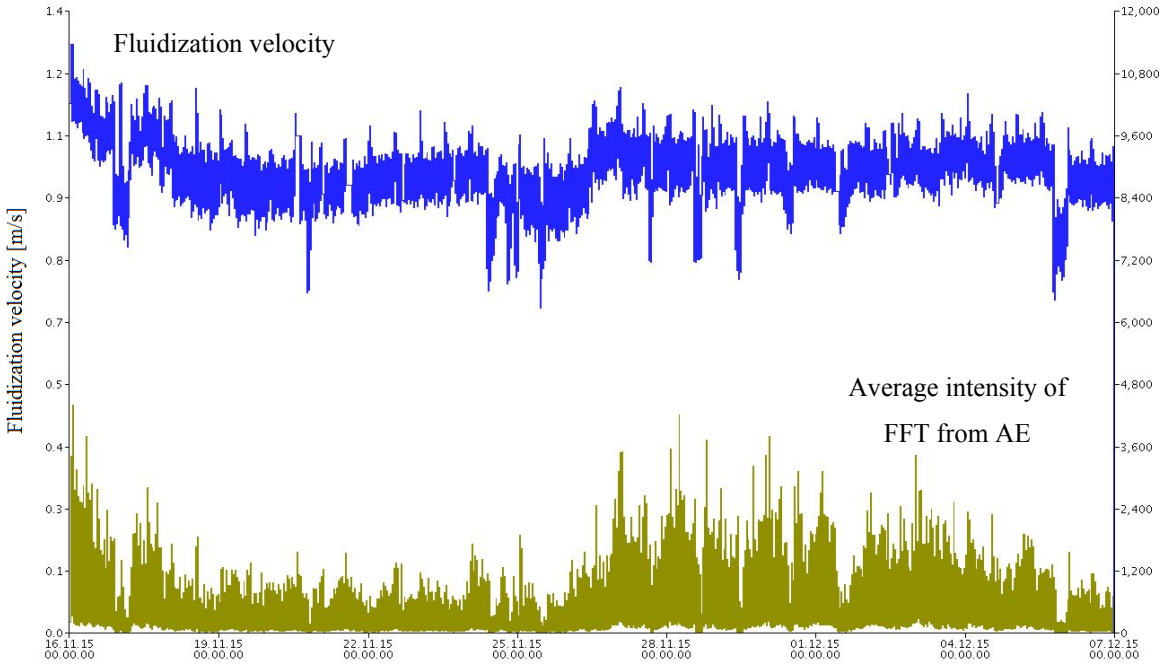

Figure 37. AE intensity of the frequency band 5 from sensor E over a time period of 21 days.

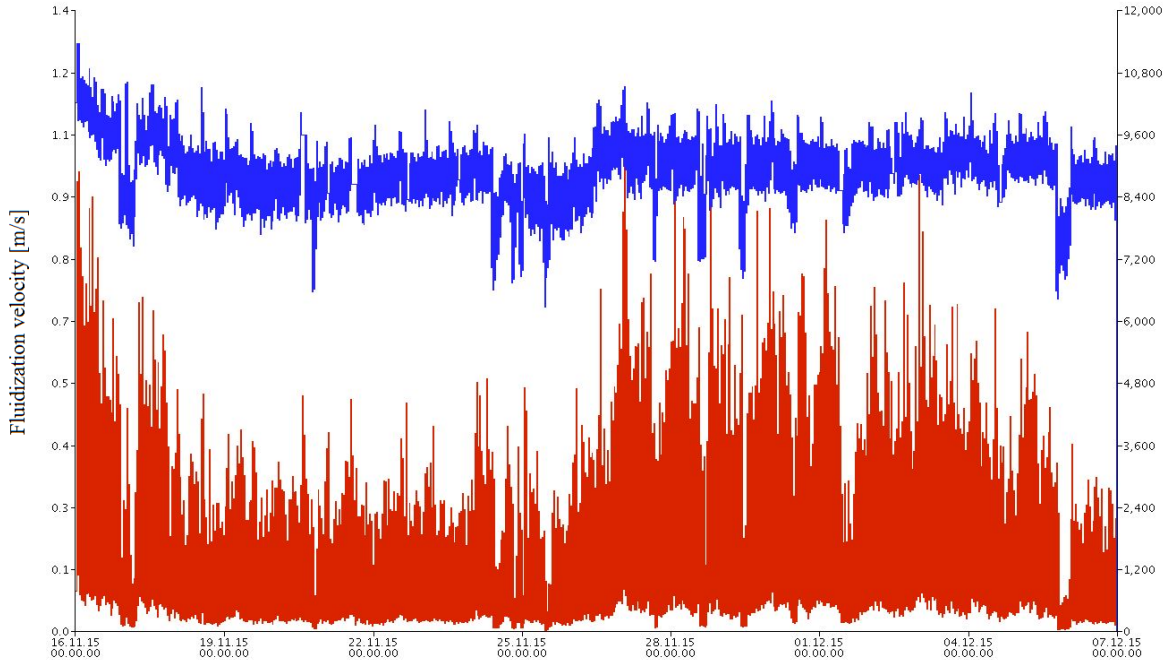

Figure 38. Fluidization velocity and AE intensity of the frequency band 2 from sensor E over a time period of 21 days.

Fluidization velocity is controlled by boiler load. As load is increased more fuel and air is fed into the furnace. As seen in the figures above, AE is sensitive to fluctuations of superficial gas flow. This observation fits the theory discussed in chapter 4. As fluidization velocity increases AE intensifies. Subtractions of different frequency bands facilitate to observe the changes of AE visually. For example the dependence between AE and fluidization velocity can be seen more clearly by looking at the subtraction trend instead of individual AE trends.

The Table 11 presents some statistics of AE data from the time of the test period. While the average value grows, range gets wider and variation increases throughout the results. Comparison between the sensors is not unambiguous because all of the rods do not have the same surface area and circumstances in different parts of the bed may vary. The sensors installed horizontally (C, D, E) give more intense AE than the sensors installed vertically (A, B) This might result from particles' up and down movement in the bed. Horizontal waveguides have also more surface area for particles to collide on. Frequency band 2 has the highest average intensity values of each sensor. Lowest average intensity values are found on frequency band 3 (sensors A and E) or 5 (sensors B, C and D). Data from

different frequency bands do not appear to alternate proportionately as conditions change. Different frequencies may reflect different events and changes.

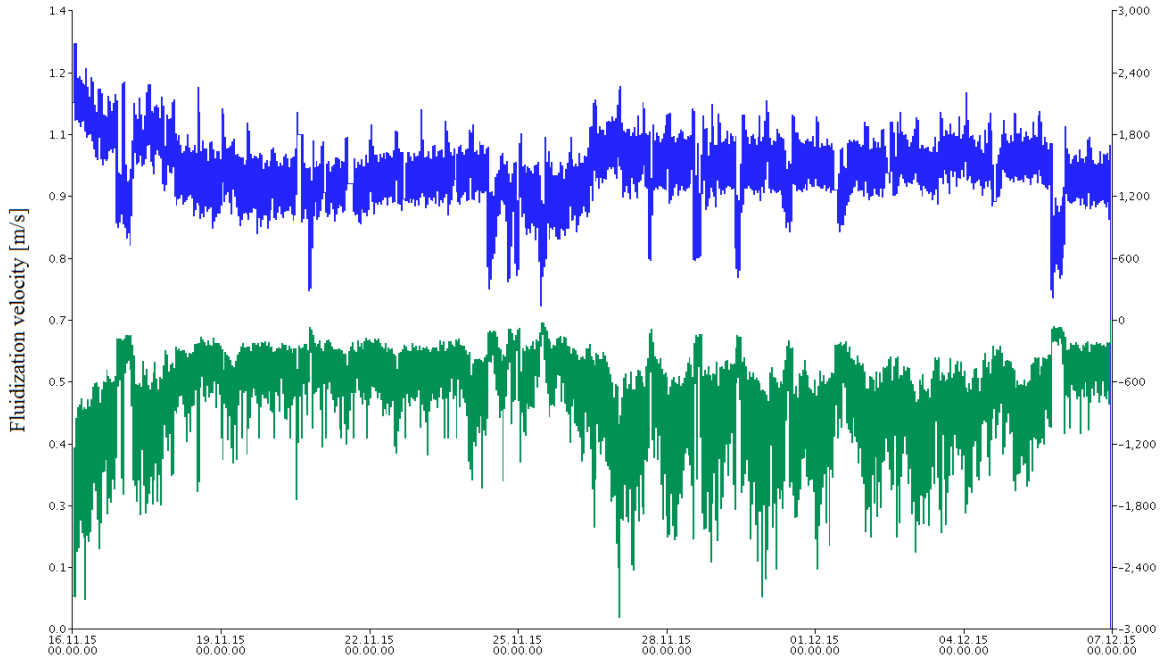

Figure 39. Subtraction of intensities of the bands 2 and 5 from previous figures is almost like a reversed image of fluidization velocity trend.

Sensor A has significantly lower intensities than other sensors. This may be the result of slagging. During shutdowns in the past it has been noticed that bed material has stack on sensor rods and especially on the rod A. It can be concluded that AE of every sensor damps in time in consequence of fouling. After every shutdown when the furnace is cleaned from local sinters, it can be assumed that the mixing of the bed returns to more even across the bed.

When focusing on the statistics of T-shaped sensors C, D and E, it can be noticed that C has the highest and E has the lowest intensity. When statistics of sensors C and D are compared, it can be noticed that intensity levels of sensor C are higher on every frequency band studied. Probably more particles collide on rod C because it is in the area where solid fuel hits the bed. Because of E-waveguide's location in the furnace, acoustic emission caused by fuel feed and its fluctuation does not affect the measuring as much as it would near the front wall. It is not clear how mixing of the bed alternates across the bed.

According to the theory of AE technology, the coarser the bed the more intensive is the intensity of acoustic emission. With the knowledge obtained over the study, no firm conclusions about coarsening of the bed can be drawn on the strength of the AE data and knowledge to interpret it.

Table 11. Statistics of AE data from time of the test period plus 40 hours (t=0 to t=120) shows the differences between the sensors and between the frequency bands.

Tag	Average intensity	Range	Standard deviation	Variance
A -1	97	856	63	3 955
A -2	182	1 703	126	15 929
A -3	54	940	50	2 461
A -4	48	1 041	46	2 113
A -5	43	855	40	1 573
B -1	644	6 262	484	234 080
B -2	1 305	11 731	1 019	1 037 691
B -3	301	4 920	317	100 322
B -4	307	4 989	329	108 063
B -5	562	7 627	555	307 605
C -1	1 395	10 004	755	570 038
C -2	2 228	13 636	1 210	1 464 775
C -3	842	7 522	548	300 690
C -4	1 022	8 862	639	408 650
C -5	1 005	7 763	602	362 259
D -1	975	4 344	425	180 324
D -2	1 571	7 681	703	494 363
D -3	488	3 293	276	76 427
D -4	532	3 407	294	86 428
D -5	815	4 588	429	183 735
E -1	705	5 931	475	225 766
E -2	937	9 139	682	465 458
E -3	361	5 700	329	108 176
E -4	424	6 034	368	135 372
E -5	300	4 205	263	68 950

7 CONCLUSIONS

When operating a bubbling fluidized bed boiler it is important to get information about the bed conditions. Alkalis in biomass fuel ash may interact and react chemically with bed material and form alkali silicates with low melting point. This results in bed clustering which can lead to total bed sintering and defluidization. Information about bed conditions during boiler operation enables early detection of agglomeration. Early detection gives the operator time to react and prevent unplanned shutdowns caused by total bed sintering. Furthermore, the information helps to prevent bed coarsening and enrichment of stones from the fuel.

Knowledge about the bed conditions enables also the optimization of bed material consumption. Bed material might be replaced just to be on the safe side and extra bed material is consumed. This is usually thought to be reasonable because shutdowns are expensive due to lost profit. Nevertheless, there are no benefits in replacing and dumping of good bed material. It causes unnecessary costs and it does not either coincide with the present-day goal of resource efficiency. An obstacle to optimization of bed material consumption has been the difficulty to acquire information about the bed conditions.

Conventional methods in monitoring of fluidized bed include visual observation and temperature and pressure control. Bubbling can be observed visually from the furnace sight glasses and bed material quality from bottom ash conveyors. There are pressure and temperature measurements in the bed. Pressure measurements reflect the hydrodynamics of the bed but do not solely give an early warning of agglomeration. Temperature measurements describe the local bed mixing even better than pressure measurements but react to changes with a longer delay.

The case study carried out at a BFB boiler included optimization of bottom ash system and sand feeding. The feasibility and potentiality of two novel systems for bed monitoring were evaluated. The systems studied were acoustic emission measurement in the bed and digital image analysis from bottom ash images taken at the conveyor. Both technologies offer tools for acquiring information about bed conditions. AE can give online information about

particle movement and hydrodynamics of the bed. Digital image analysis can give data about the particle size of bed material once it has exited the boiler.

During and following the test period consumption of fresh sand was reduced gradually and the perceived quality difference between the bottom ash from front wall and rear wall sides was balanced. This was done without endangering the steam production. Adjusting the settings was done after careful calculations and evaluation of effects the changes would cause. The sand consumption was estimated starting from three different bases. Theoretical sand feed according to sand screw running settings decreased 16 percent from the initial settings. This was estimated to produce a yearly saving of about 5000 euros which is not a huge expense for a boiler of the size at issue.

Particle size distribution of bottom ash determined by way of digital image analysis did not correspond to the results from sieving by hand. Bottom ash was coarser than expected according to the image analysis. Size distribution according to manual sieving was more reasonable. The difference between the results can derive from the following. Results from image analysis were based on the areal shares and sieving results described the percentage by weight. When the drag chain conveyor moves the pile of ash forward, it can be assumed that the coarser fraction stays on top of the pile while fine fraction sinks underneath it. Consequently, particles that appear in the images may not represent the size distribution very well. On the other hand, monitoring the amount and size of bigger particles might be enough instead of the determination of actual particle size distribution. A method designed for recognizing big particles from bottom ash images was demonstrated in chapter 5.2.

As it is stated in the literature, interpretation of AE requires expertise and experience greatly starting from the field of digital signal processing. AE-system in the case study presents the data as a continuous FFT which is split to frequency bands of interest. AE's dependence on fluidization velocity is evident when collected data is investigated. To obtain more information about the bed conditions and to notice the possible change of coarseness of the bed in AE the data requires further processing or at least comprehensive experience. Reference data together with corresponding description of process and bed conditions could help to determine and set alarms for agglomeration. The fluidizing bed at

issue has been working only too well to obtain reference data from occasions of fluidizing problems.

7.1 Research Reliability

Experimental part was performed at an industrial power plant in production which caused certain limitations and difficulties to monitoring and sampling. Tests were performed without endangering the steam production. It was not possible to search for limiting values because of the risk of severe sintering and boiler shutdown. The output of the boiler alternated during the test period more than it was expected. This resulted from changes in the steam demand. Relative to the results, it would have been best to operate the boiler on the terms of testing and collecting data. In laboratory circumstances testing would have been more accurately controlled. Results from laboratory on the other hand would have not necessarily corresponded to industrial scale.

Sampling for determining the particle size distribution could have been more comprehensive. The bed did not reach a balance state before the end of the test period. In theory, total change of bed material takes over 4 weeks when estimated from sand feeding settings. Collecting the samples of bottom ash was difficult because there was no proper connection for sampling. Because of that, one can question the representativeness of the samples. Inspection did not take the variation of bottom ash density into account. Nevertheless, particle size distributions determined by sieving were reasonable according to former knowledge.

A simplifying assumption made in the calculations was that the density of fresh sand and bottom ash were both 1500 kg/m^3. In reality, the density of bottom ash might be higher than the density of fresh sand. Bottom ash includes some stones from the fuel that increase the density. However, when the bottom ash from the boiler was visually observed, it did not contain a lot of stones. The capacities of the sand and the bottom ash screws specified by equipment supplier were used in calculations. The capacities were not tested but it can be assumed from previous knowledge that they hold up well.

There was no exact information about the condition of acoustic sensors because there was no possibility of a shutdown before the test period to inspect the bed area. It is indistinct

why one of the sensors sends data of different order of magnitude. That might result from slagging on the waveguide.

7.2 Future Research and Development

In the near future as the monitoring methods develop on, acquiring information from fluidized bed is expected to become easier and more reliable. This helps to maintain good bed quality and prevent problems in the process. It also makes optimization of bottom ash balance simpler. Neither of the systems evaluated in this study is ready as it is to serve in detection of agglomeration or bed coarsening. Both technologies do have potential but require further research and developing.

Image analysis from bottom ash could be integrated in real time into the boiler control system. Instead of particle size distribution alarm limits could be set for bigger particles and the quantity of them. Surveillance of separate particles with certain parameters could be more reliable than the analysis of the size distribution. The main advantage the digital image analysis has over other detection methods is its simplicity and low-price. Even only an online image or video from the bottom ash conveyor could tell the boiler operator significant information about changes in bed quality.

According to the literature, EARS appeared to be the most effective for industrial-scale online agglomeration detection because of its insensitivity towards fluidization velocity. A model of same kind would probably suit AE. AE technology is applicable in determination of the bed material particle size. Developing the AE measurement system would require person with knowledge about signal processing and mathematical modelling. The model to develop should be insensitive to the changing quality of solid biomass fuels as well. The best would be a single parameter that told the boiler operator the quality of the bed. AE system needs to be thoroughly designed, installed and finally adjusted with the help of reference data.

Other related subject for future research could be an extensive balance sheet calculation of the bed. What is the actual volume of solid flows leaving the bed? These flows include bottom ash and particles that escape the furnace with flue gases. What is the rate of bottom ash returning to the furnace after sieving? These balances would be boiler-specific but help

in understanding the bed conditions better. Another subject of research and model could be the chemical reactions that result in agglomeration. This kind of future research would support to develop the detection of bed agglomeration.

REFERENCES

Andritz Oy. 2016. [Internal Material].

Aura, K. 2013. Akustinen emissio (in Finnish). NDT-Days 2013. The Welding Society of Finland. NDT Committee. [Seminar material]. [retrieved January 21, 2016]. Available at: http://www.shy-hitsaus.net/LinkClick.aspx?fileticket=La2eSW7tddg%3d&tabid=4768

Bartels, M., Lin, W., Nijenhuis, J., Kapteijn, F., van Ommen, J. R. 2008. Agglomeration in fluidized beds at high temperatures: Mechanisms, detection and prevention. Progress in Energy & Combustion Science. 2008. Vol. 34(5). pp. 633–666.

Basu, P. 2006. Combustion and Gasification in Fluidized Beds. CRC Press. 2006. ISBN: 978-1-4200-0515-8.

Benes, P. & Uher, M. 2010. Measurement of Mixture Mass Ratio by Acoustic Emission Method. 29th European Conference on Acoustic Emission Testing 2010. EWGAE.

Blomberg, P. 2005. Kattilalaitoksen polttotekniikat ja ilmajärjestelmät (in Finnish). Tampereen ammattikorkeakoulu. 98 p.

Caillat, S. & Vakkilainen, E. 2013. Large-scale biomass combustion plants: an overview. Biomass Combustion Science, Technology and Engineering. Safari Books [Online-digital library]. Available at: https://www.safaribooksonline.com/library/view/biomass-combustion-science/9780857091314/xhtml/B9780857091314500091.htm (Password is compulsory)

Chen, X.M. & Chen, D.Z. 2008. Measuring Average Particle Size for Fluidized Bed Reactors by Employing Acoustic Emission Signals and Neural Networks. Chem. Eng. Technol. 2008. Vol. 31(1). pp. 95–102

FI 121557 B. 2008. Järjestely ja menetelmä leijupetireaktorin pedin tilan valvontaan ja leijupetireaktori. Andritz Oy, Helsinki, Finland. (Aura, K.) FI 20060745, 21.8.2006. Published 22.2.2008. 12 p.

Geldart, D. 1973. Types of Gas Fluidization. Powder Technology. Vol. 5(7). pp. 285–292.

Gonzalez, R.C. & Woods, R.E. 2008. Digital Image Processing. 3rd ed. Upper Saddle River (NJ): Pearson/Prentice Hall. 954 p. ISBN 0-13-505267-X.

Huhtinen, M., Kettunen, A., Nurminen, P. & Pakkanen, H. 2000. Höyrykattilatekniikka (in Finnish). 5th ed. Opetushallitus. Helsinki: Oy Edita Ab 2000. ISBN 951-37-3360-2.

Hulkkonen, S. & Kauranen, T. 2009. High performance biomass boilers for green energy production boilers. TAPPSA Journal. November, 2009. South Africa. 7 p.

Hyppänen, T. & Raiko, R. 2002. Leijupoltto (in Finnish). Poltto ja palaminen. (Raiko, R. et al.) Helsinki: Teknillistieteelliset akatemiat. ISBN 951-666-604-3. pp. 490–521.

Jähne, B. 2004. Practical Handbook on Image Processing for Scientific and Technical Applications. 2nd ed. CRC Press. ISBN 0-8493-1900-5.

Jähne, B. 2005. Digital Image Processing. 6th ed. Springer-Verlag Berlin Heidelberg. ISBN 3-540-24035-7.

Khan, A.A., de Jong, W., Jansens, P.J. & Spliethoff, H. 2008. Biomass combustion in fluidized bed boilers: Potential problems and remedies. Fuel Processing Technology. 2009. Vol. 90(1). pp. 21–50.

Korbee, R., van Ommen, J.R., Lensselink, J., Nijenhuis, J., Kiel, J.H.A., van den Bleek, C.M. 2003. Early Agglomeration Recognition System (EARS). Proceedings of the 17th International Fluidized Bed Combustion Conference. ASME.

Korbee, R., Lensselink, J., van Ommen, J.R., Nijenhuis, J., van Gemert, M., Haasnoot, K. 2004. Early Agglomeration Recognition System – EARS. From bench-scale testing to industrial prototype. Energy research Centre of the Netherlands. ECN-C--04-052.

Lempinen, V., Jönkkäri, I. & Järvelä, P. 2012. Selvitys NDT-menetelmistä (in Finnish). [retrieved December 10, 2015] Available at: http://www.miktech.fi/media/getfile.php?file=248

Liukkonen, M., Hiltunen, T. & Hiltunen, Y. 2015. Evaluation of Fluidized Bed Condition by Image Analysis and Modelling. IFAC-PapersOnLine. 2015. Vol. 48(1). pp. 892-897.

Mandø, M. 2013. Direct combustion of biomass. Biomass Combustion Science, Technology and Engineering. Safari Books Online (digital library). Available at: https://www.safaribooksonline.com/library/view/biomass-combustion-science/9780857091314/xhtml/B9780857091314500042.htm (Password is compulsory)

Moilanen, A., Nieminen M. & Alèn, R. 2002. Polttoaineiden ominaisuudet ja luokittelu (in Finnish). Poltto ja palaminen. (Raiko, R. et al.) Helsinki: Teknillistieteelliset akatemiat. ISBN 951-666-604-3. pp. 117–140.

Nijenhuis, J., Korbee, R., Lensselink, J., Kiel, J.H.A., van Ommen, J.R. 2007. A method for agglomeration detection and control in full-scale biomass fired fluidized beds. Chemical Engineering Science. Vol. 62(1–2). pp. 644–654.

OpenCV 3.1.0. Tutorial for Python. 2015. Image Processing in OpenCV. [online tutorial]. [retrieved April 18, 2016]. Available at: http://docs.opencv.org/3.1.0/d2/d96/tutorial_py_table_of_contents_imgproc.html#gsc.tab=0

OpenCV 2016. About OpenCV. [www-page]. [retrieved April 28, 2016]. Available at: http://opencv.org/about.html

Prosser, W.H. 2002. Acoustic Emission. Nondestructive Evaluation Theory, Techniques, and Applications. Peter J. Shull CRC Press. 2002. EBook. ISBN 978-0-203-91106-8.

Raiko, R. 2002. Palamisen termodynaamiset perusteet (in Finnish). Poltto ja palaminen. Helsinki: Teknillistieteelliset akatemiat. ISBN 951-666-604-3. pp. 31–59

Ren, C., Wang, J., Song, D., Jiang, B., Liao, Z. & Yang, Y. 2011. Determination of particle size distribution by multi-scale analysis of acoustic emission signals in gas-solid fluidized bed. Journal of Zhejiang University-SCIENCE A. Vol. 12(4). pp. 260–267.

Scala, F. & Chirone, R. 2005. Characterization and early detection of bed agglomeration during the fluidized bed combustion of olive husk. Energy & Fuels. 2005. Vol. 20(1). pp. 120–132.

Saastamoinen, J. 2002. Kiinteän polttoaineen palaminen ja kaasutus (in Finnish). Poltto ja palaminen. (Raiko, R. et al.) Helsinki: Teknillistieteelliset akatemiat. ISBN 951-666-604-3. pp. 186–232.

Salmenperä, P. & Miettinen, J. 2005. Akustisen emission Wavelet-analyysi. [Seminar material] [retrieved January 21, 2016]. Available at: http://virtual.vtt.fi/virtual/proj3/prognos/prognos/pdf/oulu_05_salmenper%C3%A4.pdf

Skrifvars, B.J. & Hupa, M. 2002. Tuhka, kuonaantuminen, likaantuminen ja korroosio (in Finnish). Poltto ja palaminen. (Raiko, R. et al.) Helsinki: Teknillistieteelliset akatemiat. ISBN 951-666-604-3. pp. 269–299.

Skrifvars, B.J., Yrjas, P., Laurén, T., Kinni, J., Tran, H. and Hupa, M. 2005. The Fouling Behaviour of Rice Husk Ash in Fluidized-Bed Combustion. 2. Pilot-Scale and Full-Scale Measurements. Energy & Fuels. 2005. Vol. 19(4). pp. 1512–1519.

Strömberg, B. & Herstad Svärd, S. 2012. Bränslehandboken 2012 (in Swedish). The Fuel Handbook 2012. Värmeforsk Rapport 1234. ISSN 1653-1248.

Teir, S. 2003. Steam Boiler Technology. Helsinki University of Technology, Laboratory of Energy Engineering and Environmental Protection: Picaset Oy, Helsinki. ISBN 951-22-6759-4.

Turunen, V. 2015. MS-C1420 Fourier-analyysi. [Lecture hand-out]. [retrieved March 10, 2016]. Available at: https://mycourses.aalto.fi/pluginfile.php/199090/mod_resource/content/1/fourier15s.pdf

Wang, J., Cao, Y., Jiang, X. & Yang, Y. 2009. Agglomeration Detection by Acoustic Emission (AE) Sensors in Fluidized Beds. Ind. Eng. Chem. Res. 2009. Vol. 48(7). pp. 3466–3473.